Acta Mech 229, 2923–2946 (2018)
https://doi.org/10.1007/s00707-018-2131-5

ORIGINAL PAPER

Mohil Patel · Ahmed A. Shabana

Locking alleviation in the large displacement analysis of beam elements: the strain split method

Received: 11 August 2017 / Revised: 26 December 2017 / Published online: 5 April 2018

Abstract This paper proposes a new locking alleviation technique for absolute nodal coordinate formulation (ANCF) beam and plate elements based on a strain split approach. The paper also surveys classical finite element (FE) and ANCF locking alleviation techniques discussed in the literature. Because ANCF beam elements, which allow for the cross-sectional stretch fully capture the Poisson effect, Poisson locking is an issue when such beam elements are considered. The two-dimensional fully parameterized ANCF beam element is primarily used in this investigation because such an element can serve as a good surrogate model for three-dimensional ANCF beams and plates as far as membrane, bending and transverse shearing behavior is concerned. In addition to proposing the *strain split method* (SSM) for ANCF locking alleviation, this work assesses the ANCF element performance in the cases of higher-order interpolation, enhanced assumed strain method, elastic line method, and the enhanced continuum mechanics approach, and demonstrates the design of the enhanced strain interpolation function by using the shape functions of higher-order ANCF elements. Additionally, a new higher-order ANCF two-dimensional beam element is proposed in order to compare its performance with other finite elements that require the use of other locking alleviation techniques proposed and reviewed in the paper. Finally, several numerical examples are shown to demonstrate the effectiveness of the locking alleviation methods applied to ANCF elements. The purpose of this investigation, apart from proposing a new locking alleviation technique, a new higher-order beam element, and comparing several existing locking alleviation techniques, is to show that dealing with locking in fully parameterized ANCF elements is feasible and that several methods exist to effectively improve the ANCF element performance without sacrificing important ANCF element properties and features including position vector gradient continuity. Because of the use of ANCF position vector gradients as nodal coordinates, complex stress-free initially-curved geometries can be systematically obtained. Such initially-curved geometries require special attention when attempting to solve locking problems, as will be discussed in this paper.

1 Introduction

The absolute nodal coordinate formulation (ANCF) was proposed as a new FE formulation designed for correctly and efficiently capturing large deformation and rotation effects in a non-incremental solution framework [74]. Over the past two decades, a significant amount of research has been conducted on ANCF elements and its applications. ANCF element technology includes several different types of beam, plate/shell and solid

M. Patel · A. A. Shabana (✉)
Department of Mechanical and Industrial Engineering, University of Illinois at Chicago, Chicago, IL 60607, USA
E-mail: shabana@uic.edu

M. Patel
E-mail: mpate72@uic.edu

elements based on standard polynomial basis functions [45,53,54,76,95], rational basis functions [58,71], and with rotations as degrees of freedom instead of gradient vectors [57,101]. ANCF elements have been used in a diverse range of applications like tracked vehicles, tires, satellites, and pantograph–catenary systems [28,38,41,59]. However, like classical finite elements, ANCF elements can suffer from the locking phenomenon. ANCF locking has been studied by several authors in the past, and solutions have been proposed. Detailed reviews on ANCF formulation and elements can be found in the work of Gerstmayr et al. [27] and Nachbagauer [47].

The aim of this paper is multi-fold; however, the overall focus of the work is on locking alleviation techniques in ANCF. Two-dimensional ANCF beam elements are primarily used in this work to demonstrate the effectiveness of the locking alleviation techniques proposed and discussed in this paper since they can be considered as a good surrogate to understand and quantify the membrane, bending, and transverse shear-related response of three-dimensional beam and plate elements. This paper is organized as follows: Locking alleviation techniques in the classical FE literature are reviewed and discussed in Sect. 2 in order to emphasize the fact that locking is a commonly occurring phenomenon in most FEs and can be dealt with in the case of fully parameterized ANCF elements by identifying the cause of the locking and studying previous contributions in this area. Existing ANCF locking alleviation techniques are briefly reviewed in Sect. 3, while ANCF element kinematics and the general continuum mechanics approach are briefly discussed in Sect. 4. The materials reviewed in Sect. 4 will be repeatedly used in the following sections of the paper. A new two-dimensional higher-order beam element is also proposed in Sect. 4, followed by a short discussion on the effect of constitutive model assumptions on the planar ANCF beam element. A new locking alleviation technique called the *strain split method* (SSM) is proposed in Sect. 5 for two-dimensional beam elements and is generalized for three-dimensional beam and plate elements. The enhanced continuum mechanics approach and the elastic line approach are briefly reviewed in Sect. 6. The enhanced assumed strain approach is also reviewed in Sect. 6, and a method of incorporating higher-order ANCF shape functions in lower-order beams through enhanced strains is demonstrated. Section 7 compares the locking alleviation techniques proposed and discussed in Sects. 5 and 6 using five numerical examples. These include three static and two dynamic examples. Conclusions drawn from this investigation are presented in Sect. 8.

2 Locking alleviation in classical finite elements

Because many classical finite elements suffer from locking problems, locking has been thoroughly investigated by the FE community, and numerous techniques have been proposed over the years for effectively eliminating its effect on the element solution. Some of the locking mechanisms that affect classical finite elements include shear, Poisson, curvature thickness, membrane and volumetric locking. A significant amount of literature exists for locking alleviation techniques in case of commonly used elements like the classical beam, shell, and hexahedral elements. These techniques typically include improvement in element kinematics, modification of constitutive models, usage of mixed formulations, or a specifically tailored numerical fix. This section will review some of the general locking alleviation techniques used in the classical FE theory and locking alleviation methods specifically designed for classical beams. Due to the immense amount of literature available on the topic of FE locking, only a tiny fraction of it pertaining to specific locking alleviation techniques will be presented in this section.

One of the most widely used techniques to alleviate locking is *reduced integration*, and two of the earliest investigations on this topic are by Zienkiewicz et al. [102,103] where the performances of the shell element, isoparametric quadrilateral element, and the beam element are improved. Reduced and *selective integration* was applied to plate elements by Hughes et al. [30] to alleviate shear locking in the thin regime. Malkus and Hughes [42] demonstrated the equivalence of certain mixed formulations and the displacement formulation using reduced integration and showed that reduced integrated elements can match the performance of their mixed formulation counterpart. Hughes et al. [31] used reduced integration to significantly improve the behavior of a bilinear plate element in bending applications. Noor and Peters [51] used reduced and selective integration for curved beams and discussed the equivalence and 'near equivalence' of mixed and displacement-based beam models by comparing their stiffness matrices.

The *B-bar* and the *F-bar methods* are popular strategies for dealing with volumetric locking. The B-bar method is a generalized extension of selectively reduced integration where the strain displacement matrix is split into deviatoric and dilatational parts and the dilatational part is modified to help alleviate volumetric locking [32]. The F-bar approach is similar to the B-bar approach, but also applicable in the nonlinear regime.

In the simplified F-bar approach, the deformation gradient is scaled using its determinant at the integration point and at the centroid of the element [14].

Mixed methods have been extensively used in FE literature for tackling issues, including incompressibility, excessive bending stiffness, and shear locking. Sussman and Bathe [88] used a mixed displacement and pressure formulation to alleviate volumetric locking in the incompressible regime. Pian [60] proposed a mixed element based on the Hellinger–Reissner variational principle and consistently assumed stress and displacement fields to improve the bending behavior of beams and plates. Liu et al. [40] proposed the so-called flexurally super-convergent elements which are based on the Veubeke–Hu–Washizu variational principle, showing good accuracy in coarse meshes. Dorfi and Busby [17] proposed a mixed curved composite beam element that showed good convergence for displacements and stresses. Kim and Kim [37] proposed a mixed-hybrid curved beam element with nodeless degrees of freedom that is free of locking and can accurately predict stresses. Taylor et al. [91] proposed a mixed FE method for beam and frame problems that is locking-free and has properties similar to the flexibility method. A popular locking alleviation technique that has its variational basis in mixed methods is the *enhanced assumed strain method* that was proposed by Simo and Rifai [79] and is a generalization of the method of *incompatible modes* that was proposed by Bazeley et al. [6] and studied by Wilson et al. [96] and Taylor et al. [90] for rectangular elements. The enhanced strain method was extended to geometrically nonlinear problems by Simo and Armero [78]. Furthermore, it was demonstrated that the method of incompatible modes is a special case of the enhanced strain approach [79]. The enhanced strain approach was used in [80] to improve the performance of trilinear brick elements in the nearly incompressible regime. Even though the enhanced strain technique can significantly improve the element behavior in incompressible and bending deformations, the element might exhibit hourglassing in case of large strain compression [97]. Andelfinger and Ramm [1] developed two- and three-dimensional plate and shell elements using the enhanced strain approach and showed their equivalence to the assumed stress elements based on the Hellinger–Reissner approach [61]. Stolarski and Chen [85] improved the bending behavior of the two-dimensional isoparametric quadrilateral element by studying the deformation modes of the element and enhancing the strains based on physical considerations. Schwarze and Reese [73] applied reduced integration and the enhanced strain approach to the eight-node solid-shell element and demonstrated that the element can satisfy exactly the membrane and bending patch tests. Bischoff and Romero [10] proposed a generalized method of incompatible modes which is based on a pure displacement formulation, yet its elements are equivalent to the mixed formulation-based enhanced strain elements.

There is also a significant amount of work on understanding locking in the FE literature. A seminal work on understanding locking was carried out by Babuska and Suri [3] who provided quantification for the FE tendency to exhibit locking and investigated the element robustness as certain parameters of the model approached limiting values. As a specific case of a limiting parameter, Babuska and Suri [4] investigated locking onset in two-dimensional elements as Poisson's ratio approached 0.5 and studied the robustness of h and p FE refinements. Armero [2] investigated the material instabilities of enhanced strain elements under plane strain finite deformation and expanded on locking quantification in the finite deformation range. Bathe [5] used a numerical *inf-sup test* to quantify the convergence properties of shell elements under bending deformation. According to Bathe [5], satisfaction of ellipticity, consistency, and inf-sup conditions typically means that the shell element will be robust and perform well in both membrane and bending dominated problems. Prathap and Bhashyam [64] explained locking in beams as the presence of spurious constraints related to certain deformations like pure bending in case of conventional elements which might be field-inconsistent. Prathap and Babu proposed field consistent elements by using reduced integration or *field consistent strain interpolation* [62]. Rakowski [65,66] explained the phenomena of shear locking in linear and quadratic beam elements by showing that using their shape functions leads to the solution of differential equations that are different from those arising from beam theory. Stolarski and Belytschko [84] studied shear and membrane locking in curved C^0 beam elements and demonstrated that shear and membrane locking are interrelated, reduced integration weakens the flexural-membrane coupling that exists in curved elements, and mixed curved elements could also suffer from membrane and shear locking.

Another method for tackling locking is improving the element itself. There is a significant amount of literature on beam elements where the improved element targets specific locking mechanisms. Heyliger and Reddy [29] proposed a higher-order shear-deformable beam element specifically for bending and vibration problems that can correctly account for the parabolic shear stress distribution in the cross section, thus eliminating the need for a shear correction coefficient. Lee and Sin [39] made use of curvatures as degrees of freedom in order to alleviate locking in curved beam structures and accurately represent their bending energy. The rotations and radial and tangential displacements can be retrieved from relationships between the curvature

derivatives and beam strain measures in the Lee and Sin element. Yunhua [100] used the field consistence approach to explain shear and membrane locking in low-order beam elements and consequently used the field consistence approach to improve element performance. Friedman and Kosmatka [22] developed a locking-free two-node shear-deformable beam element by using cubic and quadratic polynomials for transverse and rotational degrees of freedom, respectively, and having them satisfy Timoshenko's beam differential equations. Raveendranath et al. [67] proposed a shear-deformable curved beam element that produces no spurious constraints in thin regimes, hence showing excellent performance for thin curved beam structures. A detailed review on shear-deformable beam theory and beam elements associated with it can be found in the work of Reddy [68] and Reddy et al. [69]. Furthermore, shear and membrane locking-free beam elements can be found in the works of Prathap and Babu [63], Reddy [68], and Choi and Lim [13].

Some other methods to alleviate locking include *stress projection methods* and *stiffness scaling methods*. Belytschko et al. [7] used the mode decomposition method to remove shear and membrane locking in beam elements. The mode decomposition method which is a special case of stress projection methods essentially projects the nodal displacements on a subspace of displacements such that certain modes of deformation like inextensional bending can be correctly captured. Stolarski and Belytschko [82,83] demonstrated the equivalence of the mode decomposition method and mixed finite elements based on the Hellinger–Reissner principle. Carpenter et al. [12] utilized shear scaling factors to alleviate shear locking in C^0 beam elements by splitting the stiffness matrix into bending and shear parts and modifying the shear part using a shear scaling factor that is computed using the element material and dimensional parameters. The shear scaling factor method was also used by Tessler and Hughes [92] to accurately represent the transverse shear energy in case of plate elements. Furthermore, they demonstrated that the modified stiffness matrices remain well conditioned for almost the entire range of length-to-thickness ratios. It must be noted that shear scaling is different from the shear correction factor. The shear correction factor that was proposed by Timoshenko [93] and discussed in detail by Dong et al. [16] is a standard technique used in all lower-order beam elements in order to capture a good approximation of the shear energy within the element.

3 Locking alleviation in ANCF elements

Like classical finite elements, ANCF elements are not, in general, locking-free. The locking mechanisms affecting classical finite elements also affect ANCF elements, including shear, Poisson, curvature thickness, and volumetric locking. While this section will review some of the investigations on the quantification and alleviation of locking in ANCF elements with emphasis on beams, for a detailed review on ANCF elements and their locking mechanisms the reader may also refer to Gerstmayr et al. [27] and Nachbagauer [47].

Sopanen and Mikkola [81] studied the fully parameterized ANCF three-dimensional beam element for bending, shear, and torsional deformations using three different elastic force formulations and concluded that the element does not suffer from significant shear locking and that modifying the constitutive model for the beam element based on continuum mechanics approach can improve its performance. Schwab and Meijaard [72] compared the modal properties of the ANCF three-dimensional beam element with the classical beam element by improving the ANCF beam bending deformation through the elastic line approach and shear deformation through independent shear stress and strain fields introduced via the Hellinger–Reissner and the Veubeke–Hu–Washizu principles, respectively. Gerstmayr and Matikainen [25] developed a higher-order beam element that is of fifth order in the longitudinal direction and linear in the cross section and demonstrated improvement in the prediction of axial and shear stress when compared to the solution from a commercial FE code. Garcia-Vallejo et al. [23] explained the phenomena of curvature thickness locking and shear locking in the two-dimensional ANCF beam element by studying the kinematics of the element. Furthermore, they proposed a quadratic beam element that has good bending characteristics. Dufva et al. [18] used a mixed displacement and shear strain interpolation to alleviate the two-dimensional ANCF beam element of shear locking by considering a linear distribution of the shear deformation along the longitudinal axis and improving its bending behavior by neglecting the Poisson coupling between the longitudinal and transverse normal strains. Gerstmayr and Irschik [24] studied the axial and bending deformation of ANCF beams in detail using the elastic line approach and proposed corrections to the strain measures in order to improve element accuracy in bending deformation. Hussein et al. [34] used the elastic line approach without Poisson coupling and a Hellinger–Reissner-based independent shear stress interpolation in the dynamic analysis of stiff and thin beams. Gerstmayr et al. [26] improved the performance of the original two-dimensional

ANCF beam element by forming the elastic forces using two distinct and separate methods: the first is the enhanced continuum mechanics approach which is like selectively reduced integration and the second is based on the Reissner or Simo–Vu Quoc beam theory. In order to deal with volumetric locking in case of nearly incompressible materials, Orzechowski and Fraczek [55] resorted to selectively reduced integration and the generalized F-bar approach in the three-dimensional ANCF beam element. In the past decade, several ANCF beam elements with specific locking alleviation strategies have been proposed. Kerkkanen et al. [36] proposed a two-dimensional linear ANCF beam element and used selectively reduced integration on the shear energy in order to avoid shear locking. Sugiyama et al. [87] proposed a curved gradient deficient ANCF beam element with normal strain and curvature measures described with respect to the curved reference configuration such that tangential and radial deformations can be correctly captured. Matikainen et al. [43] improved the original ANCF beam element by introducing a trapezoidal deformation mode in the cross-sectional kinematics, thus alleviating Poisson locking. Nachbagauer et al. [48,50] proposed two- and three-dimensional linear and quadratic beam elements that used a structural mechanics approach and enhanced continuum mechanics formulation to alleviate locking. Shen et al. [77] proposed a higher-order three-dimensional ANCF beam element that had quadratic interpolation for the cross-sectional deformation. The higher-order element effectively eliminated Poisson locking and could capture the warping effect in beams. This higher-order beam element was further analyzed by Orzechowski and Shabana [56] in case of buckling, torsional deformation, and different cross-sectional geometries. Ebel et al. [19] developed and analyzed several higher-order beam elements that can completely avoid Poisson locking due to improved cross-sectional deformation and showed the efficacy of the elements via the Princeton beam experiment. Hurskainen et al. [33] developed a hybrid ANCF beam element with an independently interpolated shear deformation field and demonstrated good convergence for bending problems. Mohamed and Liu [46] developed a gradient deficient beam element that uses a combination of plane strain and elastic line approach, thus exhibiting less locking than the pure continuum mechanics approach. Locking alleviation techniques similar to those used with ANCF beam elements have also been proposed for ANCF plate/shell elements. Dmitrochenko et al. [15] extended the work of Hussein et al. [34] to three-dimensional beam and plate elements. Mikkola and Matikainen [44] extended the mixed interpolation approach to three-dimensional plate elements and demonstrated its superior performance in bending scenarios compared to the original element. Ebel et al. [20] developed higher-order plate elements that alleviate shear and Poisson locking by making use of higher-order interpolation in the cross section. Yamashita et al. [99] proposed a bilinear ANCF shell element and improved its membrane and bending behavior by using the assumed natural strain and the enhanced assumed strain approach. In case of membrane dominated problems, Sanborn et al. [70] identified the issue of curve-induced distortion and membrane locking that occurs in thin plate elements and proposed a method known as *flat mapped extension modeling* to modify the axial strain by systematically excluding the effect of the curvature. Valkeapää et al. [94] used an elastic middle surface approach which is analogous to the elastic line approach along with assumed natural strain and the enhanced assumed strain methods in order to alleviate locking in the ANCF shell element.

4 ANCF finite elements

This section briefly describes the nonlinear absolute nodal coordinate formulation (ANCF) and the continuum mechanics approach for formulating the elastic forces. This brief review presents some of the basic equations that will be used repeatedly and/or referred to in the paper. One of the contributions of this paper is to introduce a new higher-order beam element which will be used as the basis for comparison with lower-order ANCF elements. In addition to introducing this element in this section, the effect of the constitutive model selection on the behavior of the planar ANCF beam elements is also discussed.

In addition to using global nodal position vectors, ANCF has the distinguishing feature of using the position vector gradients as nodal coordinates. The position vector gradients are tangents to the element coordinate lines, and therefore, their transformation when the elements are assembled differs from the conventional coordinate transformation used in the classical FE literature. Furthermore, ANCF beams differ from their classical FE counterparts which do not allow for the cross-sectional deformations. Because of the use of the transverse gradient vectors as degrees of freedom, ANCF elements allow for the stretch of the cross section. For this reason, the Poisson effect is fully captured when ANCF elements are used, and as a consequence, ANCF beam elements may experience Poisson locking which is not observed when conventional beam elements are used, as will be discussed in Sect. 5 of this paper. The use of the gradient vectors allows for obtaining complex

geometries including initially-curved geometries that require special attention when attempting to solve the locking problem, as will be discussed in this investigation.

4.1 ANCF kinematics

In the absolute nodal coordinate formulation, the global position vector of an arbitrary point on the flexible body can be written as $\mathbf{r}(\mathbf{x}, t) = \mathbf{S}(\mathbf{x})\,\mathbf{e}(t)$, where $\mathbf{S}(\mathbf{x})$ is the matrix of shape functions and $\mathbf{e}(t)$ is the vector of nodal position and gradient vectors that are defined in the global coordinate system. Depending on the element, $\mathbf{e}(t)$ can also consist of curvature vectors. The ANCF formulation leads to a constant mass matrix and zero Coriolis and centrifugal forces. Furthermore, in order to avoid computationally expensive matrix inversion or LU decomposition, Cholesky decomposition can be applied to obtain an identity generalized mass matrix associated with the ANCF Cholesky coordinates. Over the past two decades several researchers have proposed a wide range of ANCF elements. These elements include several beam, plate/shell, hexahedral, and tetrahedral elements [75]. For ANCF elements, no distinction is made between plate and shell elements since initially curved structures can be systematically obtained using an appropriate vector of nodal coordinates in the reference configuration. The constant ANCF element mass matrix can be written as $\mathbf{M} = \int_{V_0} \rho \mathbf{S}^T \mathbf{S} \mathrm{d}V_0$, where ρ and V_0 are, respectively, the mass density and volume in the reference configuration. The ANCF generalized external force vector due to a given force $\mathbf{f}_e$ can simply be written as $\mathbf{Q}_e = \mathbf{S}(\mathbf{x})^T \mathbf{f}_e$.

4.2 General continuum mechanics approach

The general continuum mechanics approach can be used to formulate the elastic forces of the ANCF elements. Using the Green–Lagrange strain and second Piola–Kirchhoff stress tensors which are defined with respect to the reference configuration, the virtual work of the elastic forces can be written as $\delta W_k = -\int_{V_0} \boldsymbol{\sigma}_{P2} : \delta\boldsymbol{\varepsilon} \mathrm{d}V_0$ where $\boldsymbol{\sigma}_{P2}$ is the second Piola–Kirchhoff stress tensor and $\boldsymbol{\varepsilon}$ is the Green–Lagrange strain tensor. This general approach allows for incorporating any type of material and geometric nonlinearities in the FE analysis. The stress tensor $\boldsymbol{\sigma}_{P2}$ can be defined as $\boldsymbol{\sigma}_{P2} = 2(\partial U/\partial \mathbf{C}_r)$, where U is the strain energy potential function that is typically written in terms of the invariants of the right Cauchy deformation tensor $\mathbf{C}_r$, defined as $\mathbf{C}_r = \mathbf{J}^T\mathbf{J}$. [11,52,75]. Alternatively, the elastic forces can be derived directly from the strain energy potential as $\mathbf{Q}_k = (\partial U/\partial \mathbf{e})$, where $\mathbf{e}$ is the vector of nodal coordinates.

4.3 Higher-order planar beam element

One method for dealing with some locking types is using higher-order elements that have richer displacement interpolations that can capture certain important deformation modes in the element, including pure bending. The use of such higher-order elements has the advantage of being able to accurately capture complex geometries that cannot be captured with low-order elements that fail to satisfy some continuity conditions for beam-like structures where curvatures have significant effects. The ANCF two-dimensional shear-deformable beam element proposed by Omar and Shabana [54] can be considered to be a higher-order element considering the fact that there are other ANCF beam elements proposed by Nachbagauer et al. [50] in the literature that are of lower-order. The Omar and Shabana element is cubic in the longitudinal direction and linear in the transverse direction, whereas the elements proposed by Nachbagauer et al. [50] are linear in the transverse direction and linear and quadratic in the longitudinal directions. All these elements, however, suffer from severe locking when used with the general continuum mechanics approach and a nonzero Poisson ratio. One must resort to using specialized elastic force formulations like the enhanced continuum mechanics approach and the Reissner–Simo–Vu Quoc structural mechanics-based approach in order to achieve good performance from these elements. One of the main reasons for the poor performance of these elements with the general continuum mechanics approach is the linear interpolation considered in the transverse direction. As explained by Shen et al. [77] and Orzechowski and Shabana [56], the use of Hooke's law in this case leads to a stiff behavior in the element response to non-uniform strain distribution like bending. One approach explored in previous investigations is refining the displacement polynomial of the lower-order elements to be quadratic in the transverse directions to allow the element to deform in a way that correctly captures the Poisson coupling effect within the element. A new higher-order element is hence proposed here in order to explore the efficacy

of this approach in the two-dimensional analysis and to later compare the use of the higher-order element approach with other locking alleviation approaches. The higher-order element, which is quadratic in the beam transverse direction, has the following interpolating polynomial:

$$\mathbf{r} = \begin{bmatrix} a_0 + a_1 x + a_2 y + a_3 xy + a_4 x^2 + a_5 y^2 + a_6 xy^2 + a_7 x^3 \\ b_0 + b_1 x + b_2 y + b_3 xy + b_4 x^2 + b_5 y^2 + b_6 xy^2 + b_7 x^3 \end{bmatrix}. \tag{1}$$

The vector of nodal coordinates of a node i for the new higher-order element is given as $\mathbf{e}^i = \left[\mathbf{r}^{iT}\ \mathbf{r}_x^{iT}\ \mathbf{r}_y^{iT}\ \mathbf{r}_{yy}^{iT}\right]^T$, where $\mathbf{r}$ is the global position vector, $\mathbf{r}_\alpha = \partial\mathbf{r}/\partial\alpha$ is a gradient vector where $\alpha = x, y$, and $\mathbf{r}_{yy} = \partial^2\mathbf{r}/\partial y^2$ is a curvature vector. The vectors $\mathbf{r}$, $\mathbf{r}_\alpha$, $\mathbf{r}_{yy}$ are two-dimensional vectors. The shape functions for the element based on the polynomials of Eq. (1) are provided in "Appendix A.1." As can be noticed from the displacement polynomial and the shape functions, the element is quadratic in the y coordinate, and hence the normal transverse strain will no longer be constant in the y direction, allowing reducing the Poisson locking effect specifically in bending situations. This element can be considered as a special (two-dimensional) case of the three-dimensional higher-order element proposed by Shen et al. [77] and analyzed by Orzechowski and Shabana [56]. Even though the shape functions of this two-dimensional element can be considered as a subset of the set of the three-dimensional higher-order element shape functions, its performance, as will be demonstrated in the next section, is dependent on the constitutive model and on plane stress or plane strain as used in the case of linear materials.

4.4 Plane stress and plane strain assumptions

The use of the appropriate constitutive model and stress and strain conditions is important in the two-dimensional analysis of ANCF beams. The two sets of stress and strain conditions available for use with the linear constitutive model are the plane strain and the plane stress models. Plane strain assumes the strain components $\varepsilon_{zz} = \varepsilon_{xz} = \varepsilon_{yz} = 0$, whereas plane stress assumes the stress components $\sigma_{zz} = \sigma_{xz} = \sigma_{yz} = 0$ [11,52,75]. Even though several previous ANCF investigations suggest that the analyst may choose either of the two assumptions, the effect of these assumptions on ANCF element performance has not been previously investigated. This study also examines the effect of plane strain versus plane stress assumption on the ANCF two-dimensional beam elements using the general continuum mechanics approach. Since in case of a beam typically the thickness of the structure is not larger than the length, plane stress is recommended as the appropriate assumption. The effect of the constitutive model and assumed stress or strain conditions can be demonstrated by a simple example of a beam undergoing small deformation. Two types of elements are considered in this case: the original two-dimensional beam element that was proposed by Omar and Shabana [54] and the higher-order element proposed in this investigation. A cantilever beam problem is considered with material properties $E = 2 \times 10^{11}$ Pa, $\nu = 0.3$, beam length of 1 m, height of 0.01 m, and thickness of 0.01 m. The cantilever beam, shown in Fig. 1, is subjected to a vertical tip load of -10 N. The results for plane strain and plane stress static analysis on the two element types are shown in Table 1. Since this is a thin beam, the classical Euler–Bernoulli beam theory predicts the analytical vertical tip deformation to be -0.02 m.

As can be seen from Table 1, the plane stress assumption leads to accurate results with the higher-order beam element and some under-prediction of deformation with the Omar and Shabana element. The plane strain assumption on the other hand results in significant under-prediction of deformation in both beam models as they cannot achieve the analytical solution. This simple analysis demonstrates that the constitutive model and the assumed stress and strain conditions also affect the element performance and such a constitutive model, and the corresponding stress and strain conditions must be carefully selected in case of two-dimensional ANCF beam analysis.

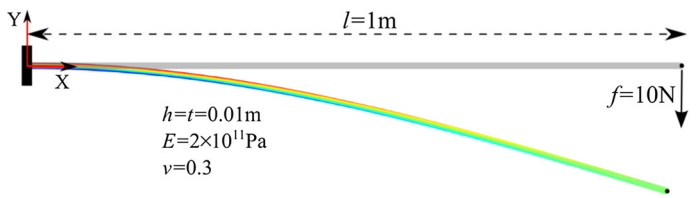

Fig. 1 Slender cantilever beam problem (deformation with respect to undeformed state is magnified for graphical purposes)

Table 1 Effect of using plane stress and plane strain (Om–Sh: Omar and Shabana beam)

Number of elements	Plane strain		Plane stress	
	Om–Sh (m)	Higher-order (m)	Om–Sh (m)	Higher-order (m)
5	−0.014690096	−0.017941054	−0.017979431	−0.019726994
10	−0.014817360	−0.018138433	−0.018148212	−0.019936221
20	−0.014845969	−0.018181342	−0.018183872	−0.019979401
50	−0.014853811	−0.018193062	−0.018193509	−0.019991023

5 ANCF strain split method

In this section, the ANCF strain split method (SSM) for solving the ANCF beam and plate locking problems is proposed and discussed. The basic differences between this method and other locking solution methods proposed in the literature will also be discussed in this paper.

5.1 Strain split method (SSM)

A new method is proposed in this study in order to address the locking problem in ANCF beams and plates. The basic idea is to analyze the element kinematics and then decouple the higher-order terms found in the axial strain and the transverse strain through an additive decomposition of the Green–Lagrange strain tensor and the constitutive law. According to the analysis performed by Sugiyama et al. [86], the two-dimensional shear-deformable beam element position field and gradients can be written, respectively, as

$$\mathbf{r} = \mathbf{r}^c + y\mathbf{r}_y, \quad \mathbf{r}_x = \mathbf{r}_x^c + y\mathbf{r}_{yx}, \quad \mathbf{r}_y = \mathbf{r}_y \tag{2}$$

where c corresponds to the centerline. Accordingly, the matrix of position vector gradients can be written as $\mathbf{J} = \left[\begin{array}{cc}\mathbf{r}_x & \mathbf{r}_y\end{array}\right] = \left[\begin{array}{cc}\mathbf{r}_x^c + y\mathbf{r}_{yx} & \mathbf{r}_y\end{array}\right]$. The matrix of position vector gradients can be additively decomposed as

$$\mathbf{J} = \left[\begin{array}{cc}\mathbf{r}_x^c & \mathbf{r}_y\end{array}\right] + \left[\begin{array}{cc}y\mathbf{r}_{yx} & \mathbf{0}\end{array}\right] = \mathbf{J}^c + \mathbf{J}^k \tag{3}$$

where $\mathbf{J}^c = \left[\begin{array}{cc}\mathbf{r}_x^c & \mathbf{r}_y\end{array}\right]$ is associated with the centerline, and $\mathbf{J}^k = \left[\begin{array}{cc}y\mathbf{r}_{yx} & \mathbf{0}\end{array}\right]$ is associated with the curvature and shear deformation of the element. Thus, the Green–Lagrange strain and the right Cauchy deformation tensors can be written, respectively, as

$$\left.\begin{array}{l}\boldsymbol{\varepsilon} = \frac{1}{2}\left[\mathbf{J}^T\mathbf{J} - \mathbf{I}\right] = \frac{1}{2}\left[\mathbf{C}_r - \mathbf{I}\right] \\ \mathbf{C}_r = \mathbf{J}^{cT}\mathbf{J}^c + \mathbf{J}^{cT}\mathbf{J}^k + \mathbf{J}^{kT}\mathbf{J}^c + \mathbf{J}^{kT}\mathbf{J}^k\end{array}\right\} \tag{4}$$

where each matrix that appears in the $\mathbf{C}_r$ expression can be written as

$$\left.\begin{array}{l}\mathbf{J}^{cT}\mathbf{J}^c = \left[\begin{array}{cc}\mathbf{r}_x^{cT}\mathbf{r}_x^c & \mathbf{r}_x^{cT}\mathbf{r}_y \\ \mathbf{r}_y^T\mathbf{r}_x^c & \mathbf{r}_y^T\mathbf{r}_y\end{array}\right], \quad \mathbf{J}^{cT}\mathbf{J}^k = \left[\begin{array}{cc}y\mathbf{r}_x^{cT}\mathbf{r}_{yx} & 0 \\ y\mathbf{r}_y^T\mathbf{r}_{yx} & 0\end{array}\right], \\ \mathbf{J}^{kT}\mathbf{J}^c = \left[\begin{array}{cc}y\mathbf{r}_{yx}^T\mathbf{r}_x^c & y\mathbf{r}_{yx}^T\mathbf{r}_y \\ 0 & 0\end{array}\right], \quad \mathbf{J}^{kT}\mathbf{J}^k = \left[\begin{array}{cc}y^2\mathbf{r}_{yx}^T\mathbf{r}_{yx} & 0 \\ 0 & 0\end{array}\right]\end{array}\right\}. \tag{5}$$

Accordingly, the strain tensor can be written as

$$\boldsymbol{\varepsilon} = \left[\begin{array}{cc}\varepsilon_{11} & \varepsilon_{12} \\ \varepsilon_{12} & \varepsilon_{22}\end{array}\right] = \frac{1}{2}\left(\left[\begin{array}{cc}\mathbf{r}_x^{cT}\mathbf{r}_x^c + 2y\mathbf{r}_x^{cT}\mathbf{r}_{yx} + y^2\mathbf{r}_{yx}^T\mathbf{r}_{yx} & \mathbf{r}_x^{cT}\mathbf{r}_y + y\mathbf{r}_{yx}^T\mathbf{r}_y \\ \mathbf{r}_y^T\mathbf{r}_x^c + y\mathbf{r}_y^T\mathbf{r}_{yx} & \mathbf{r}_y^T\mathbf{r}_y\end{array}\right] - \left[\begin{array}{cc}1 & 0 \\ 0 & 1\end{array}\right]\right). \tag{6}$$

The strain tensor can be split into two parts, one associated with the beam centerline and the other part associated with the higher-order terms that contribute to cross-sectional deformation, bending, and curvature definition

as $\boldsymbol{\varepsilon} = \boldsymbol{\varepsilon}^c + \boldsymbol{\varepsilon}^k$ where

$$\left.\begin{aligned}\boldsymbol{\varepsilon}^c &= \frac{1}{2}(\mathbf{J}^{cT}\mathbf{J}^c - \mathbf{I}) = \frac{1}{2}\left(\begin{bmatrix}\mathbf{r}_x^{cT}\mathbf{r}_x^c & \mathbf{r}_x^{cT}\mathbf{r}_y \\ \mathbf{r}_y^T\mathbf{r}_x^c & \mathbf{r}_y^T\mathbf{r}_y\end{bmatrix} - \begin{bmatrix}1 & 0 \\ 0 & 1\end{bmatrix}\right) \\ \boldsymbol{\varepsilon}^k &= \frac{1}{2}(\mathbf{J}^{cT}\mathbf{J}^k + \mathbf{J}^{kT}\mathbf{J}^c + \mathbf{J}^{kT}\mathbf{J}^k) = \frac{1}{2}\begin{bmatrix}2y\mathbf{r}_x^{cT}\mathbf{r}_{yx} + y^2\mathbf{r}_{yx}^T\mathbf{r}_{yx} & y\mathbf{r}_{yx}^T\mathbf{r}_y \\ y\mathbf{r}_y^T\mathbf{r}_{yx} & 0\end{bmatrix}\end{aligned}\right\}. \tag{7}$$

In order to alleviate locking, Poisson coupling can be used only in the lower-order terms of the normal strains that are contained in the expression of $\boldsymbol{\varepsilon}^c$. Thus, the second Piola–Kirchhoff stress can be written in Voigt form as $\boldsymbol{\sigma}_v = \mathbf{E}^c\boldsymbol{\varepsilon}_v^c + \mathbf{E}^k\boldsymbol{\varepsilon}_v^k$, where the strains are also in Voigt form. With an assumption of plane strain the matrices of elastic coefficients can be defined as

$$\mathbf{E}^c = \begin{bmatrix}\lambda + 2\mu & \lambda & 0 \\ \lambda & \lambda + 2\mu & 0 \\ 0 & 0 & \mu k_s\end{bmatrix}, \quad \mathbf{E}^k = \operatorname{diag}(E, E, \mu k_s) \tag{8}$$

where λ and μ are the Lamé parameters, E is Young's modulus, k_s is the shear correction coefficient defined as $k_s = 10(1+\nu)/(12+11\nu)$, and ν is Poisson's ratio. This leads to uncoupling of the transverse normal strain and the higher-order terms associated with bending that are contained in the longitudinal normal strain. This type of uncoupling in the deformation modes can significantly improve the element bending behavior as will be demonstrated in the numerical results section of this paper.

With regard to its treatment of the coupling between transverse normal and higher-order strains, SSM is different from locking alleviation techniques proposed in classical FE literature like the enhanced assumed strain [79] and the *free formulation* [8] that work with either element kinematics or the stiffness matrix to deal with locking. In case of the enhanced assumed strain approach, an incompatible strain field is added to the compatible strain field to improve element performance as will be discussed in Sect. 6 of this investigation. The free formulation is based on the concept of using a nonconforming *higher-order* displacement field along with the so-called *basic* displacement components which include the rigid body and constant strain element modes. The stiffness in the free formulation is written as the sum of the basic stiffness and the higher-order stiffness [21]. Furthermore, the stiffness coupling between the basic element modes and higher-order modes is modified to improve element convergence. It should be noted that this approach is different from the SSM approach since the SSM approach relies on the strain decomposition and different constitutive models to alleviate locking. In case of the free formulation, the same constitutive model is used in all stiffness calculations; hence, the method relies purely on a kinematic enhancement approach. In the conclusion of Felippa's paper [21] it is noted that the free formulation has to do with "freedom" from element conformity requirements which can help improve its performance. Since in the SSM approach no such requirement or assumption is exercised on the element in order to alleviate locking, SSM is fundamentally different from the free formulation as a locking alleviation technique.

The SSM approach is also different from the enhanced continuum mechanics approach that was proposed by Gerstmayr et al. [26] from a numerical perspective wherein the former uses full integration, whereas the latter uses selectively reduced integration as will be discussed in Sect. 6.3 of this paper. Another distinguishing SSM feature is that in the evaluation of the stress, even though it uses similar matrices of elastic coefficients, $\mathbf{E}^c$ and $\mathbf{E}^k$, that are used by the enhanced continuum mechanics approach, it uses different strain tensors, $\boldsymbol{\varepsilon}^c$ and $\boldsymbol{\varepsilon}^k$, with the given matrices of elastic coefficients.

5.2 SSM generalization

The strain split method proposed for the two-dimensional beam element can be easily extended to the three-dimensional beam and plate elements since these elements share similar features with the ANCF planar elements considered in this paper. The behavior of the spatial beam and plate elements depends on the geometry of the centerline or mid-surface and the definition of the transverse gradients. According to Sugiyama et al. [86], in case of a three-dimensional ANCF beam element, the position field and gradients can be written as

$$\left.\begin{aligned} \mathbf{r} &= \mathbf{r}^c + y\mathbf{r}_y + z\mathbf{r}_z \\ \mathbf{r}_x &= \mathbf{r}_x^c + y\mathbf{r}_{yx} + z\mathbf{r}_{zx} \\ \mathbf{r}_y &= \mathbf{r}_y, \mathbf{r}_z = \mathbf{r}_z \end{aligned}\right\}. \tag{9}$$

The matrix of position vector gradients can be written as

$$\mathbf{J} = \begin{bmatrix} \mathbf{r}_x^c + y\mathbf{r}_{yx} + z\mathbf{r}_{zx} & \mathbf{r}_y & \mathbf{r}_z \end{bmatrix} = \mathbf{J}^c + \mathbf{J}^k \tag{10}$$

where $\mathbf{J}^c = \begin{bmatrix} \mathbf{r}_x^c & \mathbf{r}_y & \mathbf{r}_z \end{bmatrix}$ and $\mathbf{J}^k = \begin{bmatrix} y\mathbf{r}_{yx} + z\mathbf{r}_{zx} & \mathbf{0} & \mathbf{0} \end{bmatrix}$. Using this split of the matrix of position vector gradients, the Green–Lagrange strain can be written as $\boldsymbol{\varepsilon} = \boldsymbol{\varepsilon}^c + \boldsymbol{\varepsilon}^k$ where

$$\boldsymbol{\varepsilon}^c = \frac{1}{2}\left(\mathbf{J}^{cT}\mathbf{J}^c - \mathbf{I}\right), \quad \boldsymbol{\varepsilon}^k = \frac{1}{2}\left(\mathbf{J}^{cT}\mathbf{J}^k + \mathbf{J}^{kT}\mathbf{J}^c + \mathbf{J}^{kT}\mathbf{J}^k\right), \tag{11}$$

and finally, the second Piola–Kirchhoff stress can be defined in Voigt form as $\boldsymbol{\sigma}_v = \mathbf{E}^c\boldsymbol{\varepsilon}_v^c + \mathbf{E}^k\boldsymbol{\varepsilon}_v^k$ where

$$\mathbf{E}^c = \begin{bmatrix} \lambda+2\mu & \lambda & \lambda & 0 & 0 & 0 \\ \lambda & \lambda+2\mu & \lambda & 0 & 0 & 0 \\ \lambda & \lambda & \lambda+2\mu & 0 & 0 & 0 \\ 0 & 0 & 0 & \mu & 0 & 0 \\ 0 & 0 & 0 & 0 & \mu k_{s2} & 0 \\ 0 & 0 & 0 & 0 & 0 & \mu k_{s3} \end{bmatrix}, \tag{12}$$

$\mathbf{E}^k = \text{diag}(E, E, E, \mu, \mu k_{s2}, \mu k_{s3})$.

In case of three-dimensional plate elements, the position field and gradients can be described using the element mid-surface and transverse gradient vector as

$$\left.\begin{aligned} \mathbf{r} &= \mathbf{r}^m + z\mathbf{r}_z, \quad \mathbf{r}_x = \mathbf{r}_x^m + z\mathbf{r}_{zx}, \\ \mathbf{r}_y &= \mathbf{r}_y^m + z\mathbf{r}_{zy}, \quad \mathbf{r}_z = \mathbf{r}_z \end{aligned}\right\}. \tag{13}$$

Accordingly, the matrix of position vector gradients and its additive split can be defined as

$$\mathbf{J} = \begin{bmatrix} \mathbf{r}_x^m + z\mathbf{r}_{zx} & \mathbf{r}_y^m + z\mathbf{r}_{zy} & \mathbf{r}_z \end{bmatrix} = \mathbf{J}^m + \mathbf{J}^k. \tag{14}$$

In this equation, $\mathbf{J}^m = \begin{bmatrix} \mathbf{r}_x^m & \mathbf{r}_y^m & \mathbf{r}_z \end{bmatrix}$ and $\mathbf{J}^k = \begin{bmatrix} z\mathbf{r}_{zx} & z\mathbf{r}_{zy} & \mathbf{0} \end{bmatrix}$. The derivation for the plate element strains and stresses follows the same procedure as discussed for the beam element.

5.3 SSM objectivity and initially curved geometry

In the case of initially curved stress-free geometry, the Green–Lagrange strain tensor can be written as $\boldsymbol{\varepsilon} = \left(\mathbf{J}^T\mathbf{J} - \mathbf{I}\right)/2$ where $\mathbf{J} = \mathbf{J}_e\mathbf{J}_0^{-1}$, $\mathbf{J}_e = \partial\mathbf{r}/\partial\mathbf{x}$, $\mathbf{J}_0 = \partial\mathbf{X}/\partial\mathbf{x}$, $\mathbf{x}$ are the element spatial coordinates in the straight configuration, $\mathbf{X} = \mathbf{S}(\mathbf{x})\,\mathbf{e}_0$ are the element parameters in the stress-free reference configuration, and $\mathbf{e}_0$ is the vector of the ANCF element coordinates in the reference configuration. Therefore, the Green–Lagrange strain tensor can be written as $\boldsymbol{\varepsilon} = \left(\mathbf{J}_0^{-T}\mathbf{J}_e^T\mathbf{J}_e\mathbf{J}_0^{-1} - \mathbf{I}\right)/2$. One can write the strain tensor in terms of the covariant strain tensor $\tilde{\boldsymbol{\varepsilon}}$ as

$$\boldsymbol{\varepsilon} = \mathbf{J}_0^{-T}\left(\frac{1}{2}\left(\mathbf{J}_e^T\mathbf{J}_e - \mathbf{J}_0^T\mathbf{J}_0\right)\right)\mathbf{J}_0^{-1} = \mathbf{J}_0^{-T}\left(\tilde{\boldsymbol{\varepsilon}}\right)\mathbf{J}_0^{-1}. \tag{15}$$

In this equation, $\tilde{\boldsymbol{\varepsilon}} = \left(\mathbf{J}_e^T\mathbf{J}_e - \mathbf{J}_0^T\mathbf{J}_0\right)/2$. The matrix of position vector gradients in the current and reference configurations can be split into centerline and higher-order parts, respectively, as $\mathbf{J}_e = \mathbf{J}_e^c + \mathbf{J}_e^k$ and $\mathbf{J}_0 = \mathbf{J}_0^c + \mathbf{J}_0^k$. Using this split, the covariant strain tensor can be written as

$$\tilde{\boldsymbol{\varepsilon}} = \frac{1}{2}\left(\left(\mathbf{J}_e^c + \mathbf{J}_e^k\right)^T\left(\mathbf{J}_e^c + \mathbf{J}_e^k\right) - \left(\mathbf{J}_0^c + \mathbf{J}_0^k\right)^T\left(\mathbf{J}_0^c + \mathbf{J}_0^k\right)\right). \tag{16}$$

Thus, $\tilde{\boldsymbol{\varepsilon}}$ can be split as the sum of two parts as $\tilde{\boldsymbol{\varepsilon}} = \tilde{\boldsymbol{\varepsilon}}^c + \tilde{\boldsymbol{\varepsilon}}^k$, where

$$\left.\begin{aligned} \tilde{\boldsymbol{\varepsilon}}^c &= \tfrac{1}{2}\left(\mathbf{J}_e^{cT}\mathbf{J}_e^c - \mathbf{J}_0^{cT}\mathbf{J}_0^c\right) \\ \tilde{\boldsymbol{\varepsilon}}^k &= \tfrac{1}{2}\left(\mathbf{J}_e^{cT}\mathbf{J}_e^k + \mathbf{J}_e^{kT}\mathbf{J}_e^c + \mathbf{J}_e^{kT}\mathbf{J}_e^k - \mathbf{J}_0^{cT}\mathbf{J}_0^k - \mathbf{J}_0^{kT}\mathbf{J}_0^c - \mathbf{J}_0^{kT}\mathbf{J}_0^k\right) \end{aligned}\right\}. \tag{17}$$

Finally, a push forward operation can be applied on the covariant strains to obtain $\boldsymbol{\varepsilon}^c$and $\boldsymbol{\varepsilon}^k$ as $\boldsymbol{\varepsilon} = \mathbf{J}_0^{-T}\left(\tilde{\boldsymbol{\varepsilon}}^c + \tilde{\boldsymbol{\varepsilon}}^k\right)\mathbf{J}_0^{-1}$, which can be written as

$$\boldsymbol{\varepsilon} = \boldsymbol{\varepsilon}^c + \boldsymbol{\varepsilon}^k \quad = \mathbf{J}_0^{-T}\left(\tilde{\boldsymbol{\varepsilon}}^c\right)\mathbf{J}_0^{-1} + \mathbf{J}_0^{-T}\left(\tilde{\boldsymbol{\varepsilon}}^k\right)\mathbf{J}_0^{-1}. \tag{18}$$

Using this SSM procedure, curved structures can be easily analyzed. This method is also applicable to straight structures as well because in straight structures $\mathbf{J}_0$ is an identity matrix and $\mathbf{J}_0^k$ is a null matrix.

In order to demonstrate that the strains remain objective, consider a rotation applied to $\mathbf{J}_e$ such that $\mathbf{J}_e^* = \mathbf{R}\mathbf{J}_e$ where $\mathbf{R}$ is a proper orthogonal rotation matrix. Consequently, $\mathbf{J}_e^*$ can be written as $\mathbf{J}_e^* = \mathbf{R}(\mathbf{J}_e^c + \mathbf{J}_e^k)$ and the covariant strains as

$$\left.\begin{aligned} \tilde{\boldsymbol{\varepsilon}}^{c*} &= \tfrac{1}{2}\left(\mathbf{J}_e^{cT}\mathbf{R}^T\mathbf{R}\mathbf{J}_e^c - \mathbf{J}_0^{cT}\mathbf{J}_0^c\right) = \tfrac{1}{2}\left(\mathbf{J}_e^{cT}\mathbf{J}_e^c - \mathbf{J}_0^{cT}\mathbf{J}_0^c\right) = \tilde{\boldsymbol{\varepsilon}}^c \\ \tilde{\boldsymbol{\varepsilon}}^{k*} &= \tfrac{1}{2}\left(\mathbf{J}_e^{cT}\mathbf{R}^T\mathbf{R}\mathbf{J}_e^k + \mathbf{J}_e^{kT}\mathbf{R}^T\mathbf{R}\mathbf{J}_e^c + \mathbf{J}_e^{kT}\mathbf{R}^T\mathbf{R}\mathbf{J}_e^k - \mathbf{J}_0^{cT}\mathbf{J}_0^k - \mathbf{J}_0^{kT}\mathbf{J}_0^c - \mathbf{J}_0^{kT}\mathbf{J}_0^k\right) \\ \tilde{\boldsymbol{\varepsilon}}^{k*} &= \tfrac{1}{2}\left(\mathbf{J}_e^{cT}\mathbf{J}_e^k + \mathbf{J}_e^{kT}\mathbf{J}_e^c + \mathbf{J}_e^{kT}\mathbf{J}_e^k - \mathbf{J}_0^{cT}\mathbf{J}_0^k - \mathbf{J}_0^{kT}\mathbf{J}_0^c - \mathbf{J}_0^{kT}\mathbf{J}_0^k\right) = \tilde{\boldsymbol{\varepsilon}}^k \end{aligned}\right\}. \tag{19}$$

That is, the strain split method does not affect the strain objectivity.

6 Other locking solution approaches

This section briefly discusses the enhanced assumed strain, elastic line, and enhanced continuum mechanics approaches used in the numerical investigation performed in this paper to compare with the SSM results. The brief description of these methods, which are well documented in literature, will shed light on the differences between different locking solution techniques. Furthermore, an enhanced strain approach based on using higher-order ANCF element shape functions with lower-order ANCF elements is demonstrated.

6.1 Enhanced assumed strain (EAS) and method of incompatible modes

The method of incompatible modes was introduced by Bazeley et al. [6] and studied by Taylor et al. [90] in order to improve the bending behavior of the classical quadrilateral element. The enhanced assumed strain approach proposed by Simo and Rifai [79] is a generalization of the method of incompatible modes. In fact Simo and Rifai [79] demonstrated that the method of incompatible modes is a special case of the enhanced assumed strain approach. In the enhanced strain approach, the incompatible strain field is defined using certain carefully designed interpolations by ensuring that the set of interpolating polynomials meets a list of conditions that are required for convergence and stability of the element. The basic idea is the enhancement of the element strain field by enriching its strain components so that its performance improves in non-uniform strain conditions. One disadvantage of this approach is the requirement of adding more variables to every element. Consider the Veubeke–Hu–Washizu energy functional in the reference configuration [9]:

$$\Pi_{\text{VHW}}(\mathbf{r}, \boldsymbol{\varepsilon}, \boldsymbol{\sigma}_{P2}) = \int_{V_0} U(\boldsymbol{\varepsilon})\,\mathrm{d}V_0 + \int_{V_0} \boldsymbol{\sigma}_{P2} : \left(\frac{1}{2}\left(\mathbf{J}^T\mathbf{J} - \mathbf{I}\right) - \boldsymbol{\varepsilon}\right)\mathrm{d}V_0 - U_{\text{ext}} \tag{20}$$

where $\boldsymbol{\sigma}_{P2}$ is the second Piola–Kirchhoff stress tensor, $\boldsymbol{\varepsilon}$ is the Lagrangian strain tensor, and U and U_{ext} are, respectively, the internal and external potential energy functions. The strain field is enhanced as $\boldsymbol{\varepsilon} = \boldsymbol{\varepsilon}^{\text{com}} + \boldsymbol{\varepsilon}^{\text{enh}}$ where $\boldsymbol{\varepsilon}^{\text{com}}$ is the compatible strain field obtained from the Green–Lagrange strain tensor, and $\boldsymbol{\varepsilon}^{\text{enh}}$ is the enhanced strain field that is element-wise discontinuous. Substituting the enhanced strain in the Veubeke–Hu–Washizu functional and making a design choice for the enhanced strain field such that $\int_{V_0} \boldsymbol{\sigma}_{P2} : \boldsymbol{\varepsilon}^{\text{enh}}\mathrm{d}V_0 = 0$ leads to

$$\Pi_{\text{VHW}}\left(\mathbf{r}, \boldsymbol{\varepsilon}^{\text{enh}}\right) = \int_{V_0} U\left(\boldsymbol{\varepsilon}^{\text{com}} + \boldsymbol{\varepsilon}^{\text{enh}}\right)\mathrm{d}V_0 - U_{\text{ext}}. \tag{21}$$

The position and enhanced strain fields can be discretized as $\mathbf{r} = \mathbf{S}(\boldsymbol{\xi})\mathbf{e}$ and $\boldsymbol{\varepsilon}^{\text{enh}} = \mathbf{M}_s(\boldsymbol{\xi})\boldsymbol{\alpha}$, where $\mathbf{M}_s$ is a shape function matrix, $\boldsymbol{\alpha}$ is a vector of additional enhanced strain variables called internal variables, $\boldsymbol{\xi} = \begin{bmatrix} \xi & \eta \end{bmatrix}^T$, $\xi = x/l$, $\eta = y/l$ are the dimensionless element parameters, and l is the length of the element. Equating the variation of the Veubeke–Hu–Washizu functional to zero leads to the following set of equations:

$$\left.\begin{aligned} \mathbf{f}(\mathbf{e}, \boldsymbol{\alpha}) &= \int_{V_0} \left(\frac{\partial \boldsymbol{\varepsilon}^{\text{com}}}{\partial \mathbf{e}} \right)^T \frac{\partial U}{\partial \boldsymbol{\varepsilon}} \mathrm{d}V_0 - \mathbf{Q}_{\text{ext}} = \mathbf{0} \\ \mathbf{g}(\mathbf{e}, \boldsymbol{\alpha}) &= \int_{V_0} \left(\frac{\partial \boldsymbol{\varepsilon}^{\text{enh}}}{\partial \boldsymbol{\alpha}} \right)^T \frac{\partial U}{\partial \boldsymbol{\varepsilon}} \mathrm{d}V_0 = \mathbf{0} \end{aligned}\right\}. \tag{22}$$

Newton's method can be used to solve the above nonlinear system of equations. After linearization, the equations used in the iterative Newton–Raphson procedure can be written in the following form:

$$\begin{bmatrix} \mathbf{K} & \mathbf{P} \\ \mathbf{S} & \mathbf{G} \end{bmatrix} \begin{bmatrix} \Delta\mathbf{e} \\ \Delta\boldsymbol{\alpha} \end{bmatrix} = - \begin{bmatrix} \mathbf{f} \\ \mathbf{g} \end{bmatrix} \tag{23}$$

where the submatrices in this equation are defined in "Appendix A.2." Alternatively, the internal variables $\boldsymbol{\alpha}$ can be eliminated at the element level using a static condensation based on the second equation of Eq. (23), $\Delta\boldsymbol{\alpha} = -\mathbf{G}^{-1}(\mathbf{g} + \mathbf{S}\Delta\mathbf{e})$, which leads to the following system of equations:

$$\left(\mathbf{K} - \mathbf{P}\mathbf{G}^{-1}\mathbf{S}\right)\Delta\mathbf{e} = -\mathbf{f} + \mathbf{P}\mathbf{G}^{-1}\mathbf{g}. \tag{24}$$

After applying the static condensation on the internal variables $\boldsymbol{\alpha}$, the equilibrium equations can be assembled for the entire mesh, the boundary conditions applied, and the resulting system is solved for $\Delta\mathbf{e}$. Once $\Delta\mathbf{e}$ is determined, $\boldsymbol{\alpha}$ can be updated for every element [78,99]. The procedure can be generalized to the dynamic case in which the element coordinates $\mathbf{e}$ are assumed known from the numerical integration. These element coordinates can be substituted into the equation $\mathbf{g}(\mathbf{e}, \boldsymbol{\alpha}) = \mathbf{0}$ which can be used to determine the internal variables $\boldsymbol{\alpha}$ to be used in the formulation of the strain energy and elastic forces. The guidelines for designing and using the enhanced strain interpolation functions are briefly reviewed in "Appendix A.3."

EAS strain interpolation

In case of the two-dimensional shear-deformable element [54], Poisson locking can cause poor convergence even after significant mesh refinement. One way to alleviate this type of FE locking (as was discussed in Sect. 4.3) is to consider a quadratic displacement interpolation in the element transverse direction that would yield a linear transverse normal strain distribution which can be sufficient to account for stiffness coupling resulting from the use of Hooke's law. Therefore, one method to achieve this type of enhancement is to consider the enhanced assumed strain interpolation to be linear in the element transverse direction. The interpolation matrix and the enhanced strain in Voigt form can be written in the parametric domain as

$$\bar{\boldsymbol{\varepsilon}}^{\text{enh}} = \bar{\mathbf{M}}\alpha = \begin{bmatrix} 0 & \eta & 0 \end{bmatrix}^T \alpha. \tag{25}$$

This leads to a linear enhancement of the transverse normal strain, and it can be shown that this type of assumed strain interpolation satisfies Eq. (A.3) because $\int_0^1 \int_{-\frac{h}{2l}}^{\frac{h}{2l}} \eta \mathrm{d}\eta \mathrm{d}\xi = 0$.

The fact that the higher-order two-dimensional ANCF beam element proposed in the preceding section is quadratic in the element transverse direction suggests using its "higher-order" shape functions as the interpolation polynomials for the enhanced strain field in order to improve the performance of the lower-order element. Keeping this concept in mind, the enhanced strain field can be assumed to be the linearized strain tensor that uses the "higher-order" shape functions that are $s_1^{\text{HO}} = l^2\left(\eta^2 - \eta^2\xi\right)/2$, $s_2^{\text{HO}} = l^2\eta^2\xi/2$. It follows that the higher-order shape function matrix can be written as $\mathbf{S}^{\text{HO}} = \begin{bmatrix} s_1^{\text{HO}}\mathbf{I} & s_2^{\text{HO}}\mathbf{I} \end{bmatrix}$, and the matrix of higher-order displacement gradients and enhanced strain tensor can be written using the element enhanced strain parameters as

$$\mathbf{J}_d^{\text{HO}} = \begin{bmatrix} \mathbf{S}_x^{\text{HO}}\boldsymbol{\alpha} & \mathbf{S}_y^{\text{HO}}\boldsymbol{\alpha} \end{bmatrix}, \quad \bar{\boldsymbol{\varepsilon}}^{\text{enh}} = \frac{1}{2}\left(\mathbf{J}_d^{\text{HO}} + \left(\mathbf{J}_d^{\text{HO}}\right)^T\right). \tag{26}$$

Furthermore, it can be shown that the enhanced strain in Voigt form can be written as

$$\bar{\boldsymbol{\varepsilon}}^{\text{enh}} = \tilde{\mathbf{M}}\boldsymbol{\alpha} = \begin{bmatrix} \mathbf{S}_{x1}^{\text{HO}} \\ \mathbf{S}_{y2}^{\text{HO}} \\ \left(\mathbf{S}_{x2}^{\text{HO}} + \mathbf{S}_{y1}^{\text{HO}}\right) \end{bmatrix} \boldsymbol{\alpha} \tag{27}$$

where $\mathbf{S}_{ab}^{\text{HO}}$ corresponds to the bth row of the matrix $\mathbf{S}_a^{\text{HO}} = \partial \mathbf{S}^{\text{HO}}/\partial a$, and $a = x, y$. One issue with this type of enhanced strain interpolation is that $\int_0^1 \int_{-\frac{h}{2l}}^{\frac{h}{2l}} s_{1,\xi}^{\text{HO}} \mathrm{d}\eta \mathrm{d}\xi \neq 0$ and $\int_0^1 \int_{-\frac{h}{2l}}^{\frac{h}{2l}} s_{2,\xi}^{\text{HO}} \mathrm{d}\eta \mathrm{d}\xi \neq 0$. This violates the condition of Eq. (A.3). In order to address this problem, the method of the constant correction matrix proposed by Ibrahimbegovic and Wilson [35] is used. The matrix of interpolating functions in the physical domain is modified by adding a constant correction matrix such that $\tilde{\mathbf{M}} = \mathbf{M}_s + \mathbf{M}_c$, where the matrix $\tilde{\mathbf{M}}$ satisfies the second part of Eq. (A.3). The correction matrix $\mathbf{M}_c$ can be defined using the equation $\int_{V_0} \mathbf{M}_s \mathrm{d}V_0 + V_0 \mathbf{M}_c = \mathbf{0}$, which leads to

$$\mathbf{M}_c = -\frac{1}{V_0} \int_{V_0} \mathbf{M}_s \mathrm{d}V_0. \tag{28}$$

In this case, $\tilde{\mathbf{M}}$ is used as the interpolation matrix to define the enhanced strain instead of $\mathbf{M}_s$ which violates Eq. (A.3).

6.2 Elastic line approach

The ANCF elastic line approach, proposed by Schwab and Meijaard [72] and used by Hussein et al. [34], can be an effective method for formulating the elastic forces for thin and stiff beams. Schwab and Meijaard [72] considered the Poisson coupling of the normal strains in their work, whereas Hussein et al. [34] did not consider this Poisson coupling. For details on the derivation of the elastic forces using the elastic line approach, the reader may refer to the publications by Schwab and Meijaard [72] and Hussein et al. [34]. A mixed method that was employed with ANCF elements in order to reduce shear locking in conjunction with the elastic line approach was the Hellinger–Reissner principle, where the shear stress field was interpolated independently within the element [34,72].

6.3 Enhanced continuum mechanics approach

As mentioned in Sect. 3, another method proposed in the ANCF literature to deal with Poisson locking is the enhanced continuum mechanics approach that was proposed by Gerstmayr et al. [26]. The roots of this method lie in the concept of classical FE selectively reduced integration. The matrix of elastic coefficients is split into two parts, one that considers Poisson coupling between the normal strains and one that does not consider this effect. While the strain split method proposed earlier in this paper is similar to the enhanced continuum mechanics approach when considering the constitutive model split, as mentioned earlier there are some fundamental differences between the two methods. In case of the enhanced continuum mechanics approach, selectively reduced integration is used, and the same strain matrix is used, for the full integration and reduced integration parts, whereas in case of the strain split method full integration is used and different strain matrices are used with two different constitutive matrices. It will be demonstrated in the numerical results section that the strain split method can be used to obtain comparable results to those of the enhanced continuum mechanics approach without the need for using reduced integration.

7 Numerical examples

In order to demonstrate and compare the effect of the locking alleviation techniques on the performance of ANCF beam elements, five numerical examples are considered: three static analysis examples and two dynamic analysis examples. The first static example is that of a slender beam subjected to small deformation. The second

Table 2 Locking alleviation technique abbreviations

Abbreviation	Type
GCM	General continuum mechanics
ECM	Enhanced continuum mechanics
EAS-1	Single parameter enhanced assumed strain
EAS-2	Higher-order shape function-based enhanced assumed strain
SSM	Strain split method
EL-SM	Schwab–Meijaard elastic line
EL-HS	Hussein et al. elastic line
ELHR-SM	Schwab–Meijaard elastic line with Hellinger Reissner shear improvement
ELHR-HS	Hussein et al. elastic line with Hellinger Reissner shear improvement
HOEL	Higher-order beam element with GCM

Table 3 Small deformation of cantilever beam static example: tip vertical displacement (m)

TYPE	5 elements	10 elements	20 elements	50 elements	100 elements
GCM	− 0.01797943	− 0.01814821	− 0.01818387	− 0.01819351	− 0.018194876
ECM	− 0.01974402	− 0.01994094	− 0.01998069	− 0.01999130	− 0.019992806
EAS-1	− 0.01974404	− 0.01994095	− 0.01998069	− 0.01999130	− 0.019992806
EAS-2	− 0.01974414	− 0.01994097	− 0.01998069	− 0.01999130	− 0.019992806
SSM	− 0.01974403	− 0.01994095	− 0.01998069	− 0.01999130	− 0.019992806
HOEL	− 0.01972699	− 0.01993622	− 0.01997940	− 0.01999102	− 0.019992674
EL-SM	− 0.01974323	− 0.01994464	− 0.01998333	− 0.01999130	− 0.019991743
EL-HS	− 0.01974800	− 0.01994487	− 0.01998334	− 0.01999130	− 0.019991743
ELHR-SM	− 0.01973830	− 0.01993950	− 0.01997930	− 0.01998984	− 0.019991308
ELHR-HS	− 0.01974306	− 0.01993973	− 0.01997931	− 0.01998984	− 0.019991308
Analytical			− 0.02		

static example is a thick beam subjected to large deformation. The third static example is that of a curved beam subjected to large deformation. The first dynamic analysis example is a two-dimensional beam pendulum subjected to gravity loading. The second dynamic analysis example is a three-dimensional cantilever beam structure subjected to gravity loading. Because all the static examples are planar, the plane stress assumption is used in all static analyses. Table 2 provides appropriate abbreviations that will be used to refer to different locking alleviation techniques. All locking alleviation techniques in Table 2 with the exception of HOEL are used with the Omar and Shabana (referred to as Om–Sh henceforth) beam element. HOEL refers to the higher-order beam element proposed in this paper in Sect. 4.3. In all the examples, the shear correction factor is used with the Om–Sh beam element and not with HOEL since HOEL has quadratic transverse interpolation, unless specified otherwise.

7.1 Slender beam: small deformation

A slender cantilever beam subjected to a vertical tip force is considered with the same element dimensions and material properties as those of the problem described in Sect. 4.4. As was mentioned previously, the analytical solution is known in this case from the classical Euler–Bernoulli theory and is calculated to be −0.02 m. The results for the static analysis are reported in Table 3 which shows the converged beam tip vertical displacement. As can be seen from these results, the Om–Sh beam element with general continuum mechanics approach cannot converge to the correct solution due to excessive stiffness resulting from Poisson locking. All the other cases can converge to the correct solution. The enhanced continuum mechanics approach, EAS-1, EAS-2, and the strain split approach show almost identical convergence in this small deformation case. Based on the results reported in Table 3, the Hellinger–Reissner principle did not improve the convergence or the solution.

7.2 Thick beam: large deformation

A thick beam example undergoing large deformation, shown in Fig. 2, is considered. The beam structure is 2 m long and has a cross section that is 0.5 m high and 0.1 m wide. The modulus of elasticity is assumed as

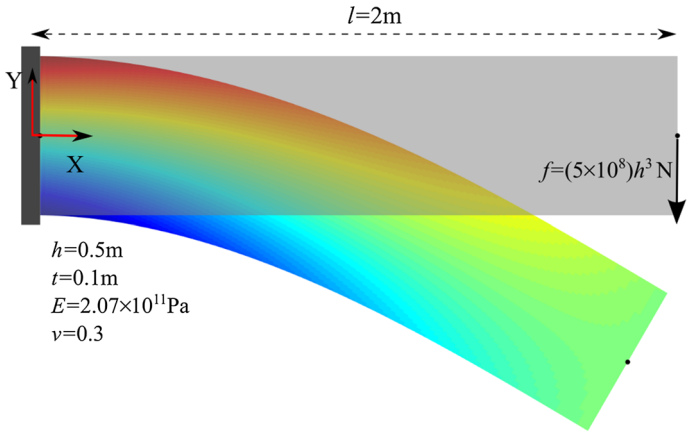

Fig. 2 Thick cantilever beam problem (actual deformation shown with respect to undeformed state)

Table 4 Large deformation of cantilever beam static example: tip vertical displacement (m)

TYPE	5 elements	10 elements	20 elements	50 elements	100 elements
GCM	−0.65915558	−0.66424157	−0.66567545	−0.66620894	−0.66633102
ECM	−0.70648069	−0.71210192	−0.71364032	−0.71421138	−0.71434336
EAS-1	−0.70749271	−0.71303640	−0.71458220	−0.71516154	−0.71529576
EAS-2	−0.70914733	−0.71423843	−0.71582370	–	–
SSM	−0.70703906	−0.71261927	−0.71416020	−0.71473509	−0.71486816
HOEL	−0.69531347	−0.70527450	−0.70867124	−0.70994038	−0.71018834
EL-SM	−0.68327030	−0.68431265	−0.68437627	−0.68439711	−0.68440429
EL-HS	−0.68356363	−0.68475960	−0.68484925	−0.68487219	−0.68487886
ANSYS			−0.713420 (converged)		

$E = 2.07 \times 10^{11}$ Pa, and Poisson's ratio is assumed $\nu = 0.3$. A fully clamped boundary condition is applied at the left end of the beam, whereas a vertical force of $-5 \times 10^8 \times h^3$ N is applied to the right end. For this example, the curvature degrees of freedom at the beam clamped end are also constrained in case of the higher-order beam element due to the large deformation nature of the problem and large cross section which could lead to significant cross-sectional deformation at the clamped end. The results of a static analysis reported in Table 4 show the converged beam tip vertical displacement. The reference solution of −0.71342 m, obtained using a commercial FE code, was achieved with 10,000 quadratic quadrilateral elements.

As can be seen from Table 4, the general continuum mechanics approach without locking alleviation converges to the incorrect solution. The higher-order beam element, enhanced continuum mechanics approach, SSM, and the EAS-1 approach can successfully alleviate locking in this example. The EAS-2 method, however, failed to converge when more than 25 elements are used. It was observed that as the element length-to-height ratio significantly decreases, numerical instabilities similar to spurious modes or hourglassing were observed when the EAS-2 method is used with the thick beam example. Recall that EAS-2 makes use of the correction matrix along with the enhanced strain formulation. A possible explanation for this phenomenon is the ill-conditioning of the stiffness matrix caused by correction matrices as the element ratio approaches zero. Such numerical instability was not seen in the EAS-2 method in case of relatively thin beams. The critical element length-to-height ratio is found to be around 0.15 for the EAS-2 method in this specific example. It should be reported that if the height of the beam in this example was reduced to 0.1 m, the numerical instability disappeared in the EAS-2 method for meshes which have more than 25 elements. A similar type of numerical instability was reported by Sussman and Bathe [89] when using incompatible mode elements in the case of geometrically nonlinear analyses and small strain conditions.

7.3 Initially curved beam: large deformation

An initially curved beam structure is subjected to large deformation in this numerical example as shown in Fig. 3. The beam is clamped at one end, and a constant tip force is applied in the global X direction. The value

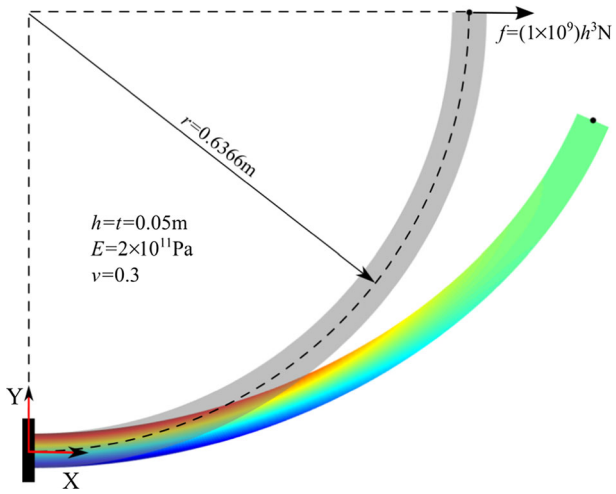

Fig. 3 Curved cantilever beam problem (actual deformation shown with respect to undeformed state)

Table 5 Large deformation of curved cantilever beam static example: tip X displacement (m)

TYPE	5 elements	10 elements	20 elements	50 elements	100 elements
GCM	0.15338680	0.16172381	0.16199009	0.16196139	0.16195412
ECM	0.16989437	0.17938015	0.17974234	0.17972820	0.17972255
EAS-1	0.16295031	0.17215697	0.17250459	0.17249109	0.17248574
EAS-2	0.16311305	0.17225897	0.17263943	0.17271119	0.17273819
SSM	0.16988736	0.17937894	0.17974213	0.17972815	0.17972252
HOEL	0.16298605	0.17213835	0.17247560	0.17246368	0.17246014
ECM-L	0.16409531	0.17247265	0.17258737	0.17250808	0.17249346
SSM-L	0.16408860	0.17247216	0.17258704	0.17250726	0.17249244
ANSYS			0.17291 (converged)		

of the force is $1 \times 10^9 \times h^3$ N. The initially curved beam arc length is 1 m, and the arc radius is 0.6366 m. The beam height and width are 0.05 m each. The material properties are $E = 2.0 \times 10^{11}$ Pa, $\nu = 0.3$, and $k_s = 1$. The results from the static analysis are shown in Table 5 which shows the beam tip horizontal displacement. The reference solution of 0.17291 m was obtained using a commercial FE code with 1000 classical beam element mesh. The ANCF higher-order beam element, EAS-1 and EAS-2 methods can converge close to the reference solution. Significant locking is observed in the beam with the general continuum mechanics approach. The strain split and enhanced continuum mechanics methods slightly overpredict the deformation. The reason for this is the loss of the constitutive coupling that occurs in curved structures between higher-order longitudinal strain terms and transverse normal strain. Such a type of coupling is fully present in the general continuum mechanics approach which is used with the ANCF higher-order beam element. One remedy to avoid the overprediction of the solution in case of the strain split method for curved structures is the consideration of coupling coefficients in the $\mathbf{E}^k$ matrix that could represent weak coupling between the higher-order longitudinal and transverse normal strains; however, it is still not yet clear how to determine such coupling coefficients for the strain split method. For example, if the $\mathbf{E}^k$ matrix is modified such that $\mathbf{E}^k(1,2) = \mathbf{E}^k(2,1) = E\nu$, the SSM converged solution is 0.1705 m, which is an improvement compared to the solution obtained without modifying $\mathbf{E}^k$.

A more effective method for improving the performance of the strain split and enhanced continuum mechanics methods in case of initially curved structures is based on giving a "local" meaning to the constitutive model used in the SSM and ECM approaches. This entails the transformation of either the constitutive coefficients into the global frame with the understanding that the constitutive coefficients are defined with respect to the element local frame or carry out strain and stress transformations between the global and element local frames [49]. Since the transformation of the constitutive coefficients is rather cumbersome, the Green–Lagrange strain tensor used in the ECM approach and the $\boldsymbol{\varepsilon}^c$ and $\boldsymbol{\varepsilon}^k$ strain matrices used with the SSM approach can be first transformed into the element local frame, the local stress can be evaluated within this element frame, and then the resulting local stress can be transformed back into the global frame in order to evaluate the element

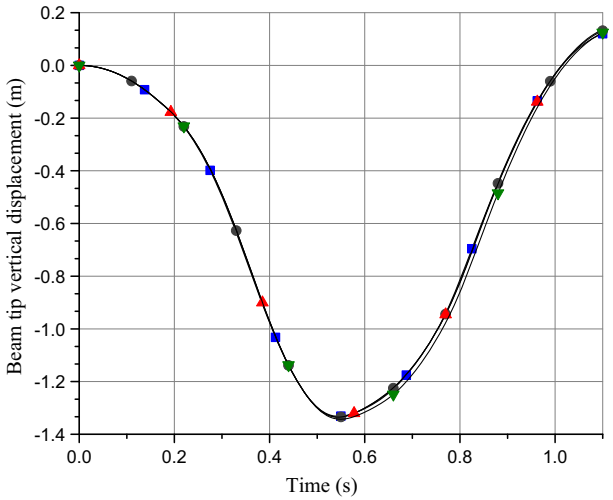

Fig. 4 Comparison of beam tip vertical displacement for different formulations in case of plane stress (—■— GCM, —●— ECM, —▲— SSM, —▼— HOEL)

elastic forces [49]. Using such a procedure, the SSM and ECM techniques yield accurate results for initially curved structures as can be seen in Table 5, where the results for the two approaches are labeled as SSM-L and ECM-L referring to the local interpretation of the constitutive model used. A tangent element frame can be defined in case of ANCF beam elements at the first node as $\mathbf{A} = \left[\mathbf{i}\ \tilde{\mathbf{I}}\mathbf{i}\right]$, where $\mathbf{i} = \mathbf{r}_x/|\mathbf{r}_x|$, and $\tilde{\mathbf{I}} = \left[\mathbf{a}_1\ \mathbf{a}_2\right]$, $\mathbf{a}_1 = \left[0\ 1\right]^T$, $\mathbf{a}_2 = \left[-1\ 0\right]^T$. Similarly, a cross-sectional element frame can be defined as $\mathbf{A} = \left[-\tilde{\mathbf{I}}\mathbf{j}\quad \mathbf{j}\right]$, where $\mathbf{j} = \mathbf{r}_y/|\mathbf{r}_y|$. These frames are defined using the beam reference configuration and hence do not change with time. It was observed that using either tangent frame or cross-sectional frame did not make significant difference for the problem under investigation. In case of using the local interpretation for the constitutive model, the coupling coefficients in the $\mathbf{E}^k$ matrix discussed previously are no longer required. Furthermore, the local frame is also more appropriate to use with shear correction factors used with beams. It must also be reported that the softening of the beam in case of initially curved structures discussed earlier is dependent on the beam radius of curvature, that is, less softening for a larger radius of curvature in case of SSM.

7.4 Dynamic analysis: pendulum problem

A dynamic example is presented in order to demonstrate that the newly proposed strain split method can contribute to locking alleviation in dynamic problems as well. A beam pendulum meshed with 30 elements is considered, with a length of 1 m, height of 0.25298 m, and a width of 0.00632 m as was presented in [54]. The material properties of the pendulum are $E = 7.0 \times 10^5$ Pa, $\nu = 0.3$, and $\rho = 5540\,\text{kg/m}^3$. Gravity load is considered to be the external force in this problem, and an assumption of plane stress was used in the analysis. The vertical displacement of the beam tip is shown as a function of time in Fig. 4.

The Om–Sh element with general continuum mechanics approach, the strain split method, the enhanced continuum mechanics approach, and the proposed ANCF higher-order beam element are compared in Fig. 4. Results show good convergence between different models for a dynamic analysis. The deformation seen in the higher-order element model is slightly larger than the other models since this element has curvature coordinates that add additional cross-sectional flexibility to the element. Figure 5 shows the results of the beam tip vertical displacement obtained using the general continuum mechanics approach and the strain split method using the plane strain assumptions and the Om–Sh element. The effect of locking is more evident in case of plane strain with the general continuum mechanics approach. Figure 6 shows the beam configurations at different times during the plane strain dynamic analysis. The colored beam in Fig. 6 shows the axial strain in case of the strain split model, whereas the gray beam shows the configuration of the beam obtained using the general continuum mechanics approach.

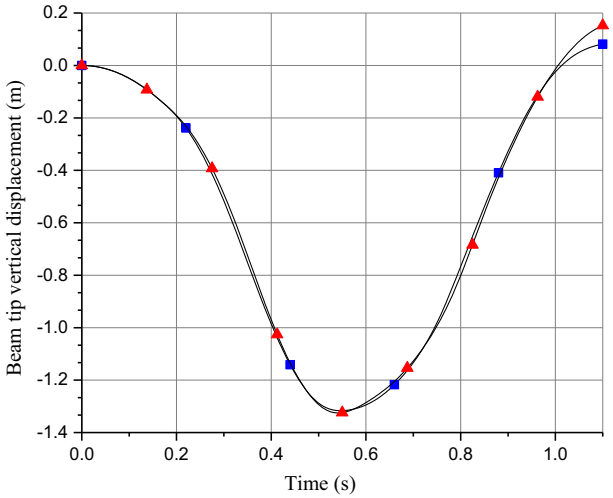

Fig. 5 Comparison of beam tip vertical displacement between general continuum mechanics and strain split method with plane strain assumption (—■— GCM, —▲— SSM)

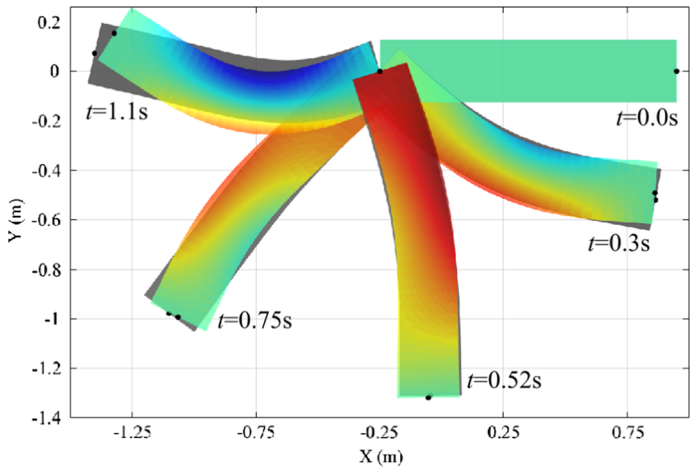

Fig. 6 Graphical representation of the pendulum motion in case of plane strain (gray: GCM; colored: SSM with axial strain contours) (color figure online)

7.5 Three-dimensional dynamic analysis: cantilever beam

Finally, a dynamic analysis of a three-dimensional cantilever beam structure is presented. This problem is identical to the one considered by Orzechowski and Shabana [56] where they compared the ANCF beam element [98] with the Shen et al. [77] higher-order beam element. The higher-order three-dimensional beam element does not have the locking seen in the relatively lower-order Yakoub and Shabana element. The beam structure length is 1 m, and the cross section height and thickness are 0.1 and 0.07 m, respectively. The material properties considered are $E = 60 \times 10^6$ Pa, $\nu = 0.3$, and $\rho = 7200\,\text{kg/m}^3$. Gravity loading is considered as external force. Figure 7 shows the beam reference and deformed configurations.

Figure 8 compares the Yakoub and Shabana element with the general continuum mechanics approach, strain split method, and the elastic line approach to the solution obtained from the higher-order Shen et al. element that used the general continuum mechanics approach. A mesh of 10 elements is considered for all models shown in Fig. 8. It can be seen from the results presented in Fig. 8 that the lower-order element with general continuum mechanics approach exhibits significant locking, whereas the other models compare well with the higher-order three-dimensional beam element. This example also demonstrates the effectiveness of the strain split method in three-dimensional beam elements. The elastic line approach gives good results in this case since the beam cross-sectional dimensions are much smaller than its length.

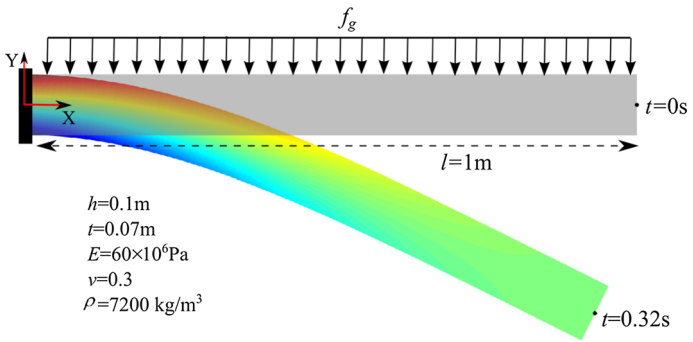

Fig. 7 Three-dimensional cantilever beam dynamic analysis (gray: beam configuration at $t = 0$ s; colored: beam configuration with axial strain contours at $t = 0.32$ s) (color figure online)

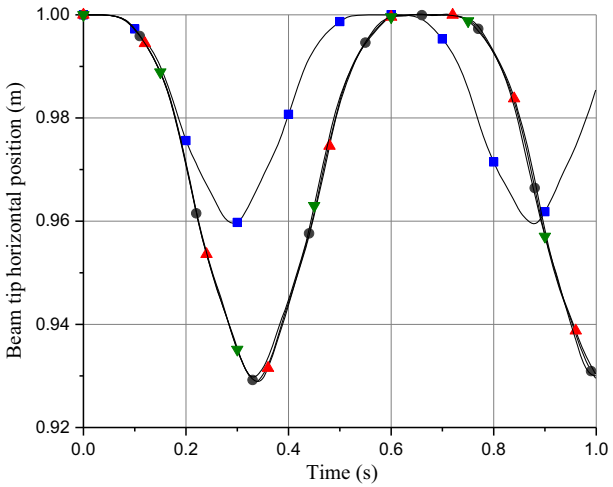

Fig. 8 Comparison of cantilever beam tip horizontal position for different models (—■— Yakoub and Shabana beam with GCM, —●— Yakoub and Shabana beam with SSM, —▲— higher-order Shen et al. beam with GCM, —▼— Yakoub and Shabana beam with elastic line approach)

8 Conclusions

The ANCF beam element locking was the subject of this paper which presented a literature review of classical FE and ANCF locking alleviation techniques. This literature review shows the significant contributions reported in the FE literature and clearly demonstrates that, while locking is a common problem in most FEs, it can be dealt with relatively easily and effectively. ANCF locking alleviation techniques can be broadly classified into two distinct categories: kinematics- and kinetics-based methods. Kinematics-based locking alleviation techniques alter the kinematic description of the element in order to improve its performance. Such methods include improvement in the displacement polynomials or improvement in the strain measures. Kinetics-based methods operate at the elastic force level by modifying the stresses without directly affecting the basic element kinematics. Such methods include different formulations of the strain energy function and reduced integration. The locking alleviation techniques investigated and compared in this paper can be categorized in the aforementioned two types. These include the new method that is proposed in this work to solve the ANCF beam and plate locking problems, known as the strain split method (SSM). A new higher-order two-dimensional ANCF beam element was also developed for the purpose of comparison with other locking alleviation methods. Implementation of the enhanced assumed strain method in ANCF beams using one parameter interpolation and using ANCF higher-order beam shape functions was presented and discussed. Three planar static examples that include a slender beam, a thick beam, and a curved beam structure undergoing small and large deformations, one planar dynamic pendulum problem and one three-dimensional dynamic cantilever beam problem were presented, and the locking alleviation techniques were compared. The newly proposed SSM concept in curved structures was discussed, and its advantages and drawbacks were discussed.

Appendix A

A.1 Higher-order ANCF planar element shape functions

The shape functions for the new higher-order two-dimensional element proposed in Sect. 4.3 are given as:

$$\left.\begin{aligned} &s_1 = 1 - 3\xi^2 + 2\xi^3, \quad s_2 = l\left(\xi - 2\xi^2 + \xi^3\right), \quad s_3 = l\left(\eta - \eta\xi\right), \\ &s_4 = \tfrac{l^2}{2}\left(\eta^2 - \eta^2\xi\right), \quad s_5 = 3\xi^2 - 2\xi^3, \quad s_6 = l\left(-\xi^2 + \xi^3\right), \\ &s_7 = l\eta\xi, \quad s_8 = \tfrac{l^2}{2}\eta^2\xi \end{aligned}\right\} \tag{A.1}$$

where $\xi = x/l$, $\eta = y/l$ are the dimensionless element parameters and l is the element length. The matrix of shape functions can be written as $\mathbf{S} = \left[s_1\mathbf{I}\ s_2\mathbf{I}\ s_3\mathbf{I}\ s_4\mathbf{I}\ s_5\mathbf{I}\ s_6\mathbf{I}\ s_7\mathbf{I}\ s_8\mathbf{I}\right]$.

A.2 Enhanced strain submatrices

The submatrices used in Eq. (23) are given as follows:

$$\left.\begin{aligned} &\mathbf{K} = \frac{\partial \mathbf{f}}{\partial \mathbf{e}} = \int_{V_0} \left(\frac{\partial \boldsymbol{\varepsilon}^{\text{com}}}{\partial \mathbf{e}}\right)^T \frac{\partial^2 U}{\partial \boldsymbol{\varepsilon}^2} \left(\frac{\partial \boldsymbol{\varepsilon}^{\text{com}}}{\partial \mathbf{e}}\right) \mathrm{d}V_0 + \int_{V_0} \left(\frac{\partial^2 \boldsymbol{\varepsilon}^{\text{com}}}{\partial \mathbf{e}^2}\right)^T \frac{\partial U}{\partial \boldsymbol{\varepsilon}} \mathrm{d}V_0, \\ &\mathbf{P} = \frac{\partial \mathbf{f}}{\partial \boldsymbol{\alpha}} = \int_{V_0} \left(\frac{\partial \boldsymbol{\varepsilon}^{\text{com}}}{\partial \mathbf{e}}\right)^T \frac{\partial^2 U}{\partial \boldsymbol{\varepsilon}^2} \left(\frac{\partial \boldsymbol{\varepsilon}^{\text{enh}}}{\partial \boldsymbol{\alpha}}\right) \mathrm{d}V_0, \quad \mathbf{S} = \frac{\partial \mathbf{g}}{\partial \mathbf{e}} = \int_{V_0} \left(\frac{\partial \boldsymbol{\varepsilon}^{\text{enh}}}{\partial \boldsymbol{\alpha}}\right)^T \frac{\partial^2 U}{\partial \boldsymbol{\varepsilon}^2} \left(\frac{\partial \boldsymbol{\varepsilon}^{\text{com}}}{\partial \mathbf{e}}\right) \mathrm{d}V_0, \\ &\mathbf{G} = \frac{\partial \mathbf{g}}{\partial \boldsymbol{\alpha}} = \int_{V_0} \left(\frac{\partial \boldsymbol{\varepsilon}^{\text{enh}}}{\partial \boldsymbol{\alpha}}\right)^T \frac{\partial^2 U}{\partial \boldsymbol{\varepsilon}^2} \left(\frac{\partial \boldsymbol{\varepsilon}^{\text{enh}}}{\partial \boldsymbol{\alpha}}\right) \mathrm{d}V_0 \end{aligned}\right\}. \tag{A.2}$$

A.3 Design of enhanced strain field

In a state of constant stress or a patch test, $\int_{V_0} \boldsymbol{\sigma}_{P2} : \boldsymbol{\varepsilon}^{\text{enh}} \mathrm{d}V_0 = 0$ must be satisfied. This leads to the following expression:

$$\int_{\Omega} \bar{\mathbf{M}} \mathrm{d}\Omega = \mathbf{0}, \quad \int_{V_0} \mathbf{M}_s \mathrm{d}V_0 = \mathbf{0} \tag{A.3}$$

where Ω is the element parametric domain, $\bar{\mathbf{M}}$ and $\mathbf{M}_s$ is the matrix of enhanced strain interpolation functions defined in the parametric domain and physical reference domain, respectively. Satisfying Eq. (A.3) is important for the stability and convergence properties of the enhanced strain-based element. Furthermore, another condition required for element stability is that the intersection of the subspaces spanned by the compatible and enhanced strain fields must be a null set. Finally, in order to ensure that the objectivity of the strain tensor is ensured, the enhanced strain interpolation functions must demonstrate frame invariance in the parametric domain [78]. The enhanced strain field interpolation functions defined in the parametric domain can be transformed into the reference domain using the following operation: $\mathbf{M}_s = (|\mathbf{J}_c|/|\mathbf{J}|)\, \mathbf{T}_c^{-T} \bar{\mathbf{M}}$ where $\mathbf{J}$ is the matrix of position vector gradients at the integration point in the reference configuration [79], c represents element coordinates corresponding to the center of the element, and the transformation matrix $\mathbf{T}$ is given as [1]

$$\mathbf{T} = \begin{bmatrix} J_{11}J_{11} & J_{12}J_{12} & 2J_{11}J_{12} \\ J_{21}J_{21} & J_{22}J_{22} & 2J_{21}J_{22} \\ J_{11}J_{21} & J_{12}J_{22} & J_{11}J_{22} + J_{12}J_{21} \end{bmatrix} \tag{A.4}$$

where J_{ij} is the ijth element of the matrix of position vector gradients defined in the reference configuration.

References

1. Andelfinger, U., Ramm, E.: EAS-elements for two-dimensional, three-dimensional, plate and shell structures and their equivalence to HR-elements. Int. J. Numer. Methods Eng. **36**(8), 1311–1337 (1993)
2. Armero, F.: On the locking and stability of finite elements in finite deformation plane strain problems. Comput. Struct. **75**(3), 261–290 (2000)
3. Babuska, I., Suri, M.: Locking effects in the finite element approximation of elasticity problems. Numer. Math. **62**(1), 439–463 (1992)
4. Babuska, I., Suri, M.: On locking and robustness in the finite element method. SIAM J. Numer. Anal. **29**(5), 1261–1293 (1992)
5. Bathe, K.J.: The inf-sup condition and its evaluation for mixed finite element methods. Comput. Struct. **79**(2), 243–252 (2001)
6. Bazeley, G.P., Cheung, Y.K., Irons, B.M., Zienkiewicz, O.C. (1965) Triangular elements in plate bending—conforming and nonconforming solutions. In: Proceedings of First Conference on Matrix Methods in Structural Mechanics, Wright-Patterson ATBFB, Ohio
7. Belytschko, T., Stolarski, H., Liu, W.K., Carpenter, N., Ong, J.S.J.: Stress projection for membrane and shear locking in shell finite elements. Comput. Methods Appl. Mech. Eng. **51**(1–3), 221–258 (1985)
8. Bergan, P.G., Nygard, M.K.: Finite elements with increased freedom in choosing shape functions. Int. J. Numer. Meth. Eng. **20**(4), 643–663 (1984)
9. Bischoff, M., Ramm, E.: Shear deformable shell elements for large strains and rotations. Int. J. Numer. Meth. Eng. **40**(23), 4427–4449 (1997)
10. Bischoff, M., Romero, I.: A generalization of the method of incompatible modes. Int. J. Numer. Methods Eng. **69**(9), 1851–1868 (2007)
11. Bonet, J., Wood, R.D.: Nonlinear Continuum Mechanics for Finite Element Analysis. Cambridge University Press, Cambridge (1997)
12. Carpenter, N., Belytschko, T., Stolarski, H.: Locking and shear scaling factors in C^0 bending elements. Comput. Struct. **22**(1), 39–52 (1986)
13. Choi, J., Lim, J.: General curved beam elements based on the assumed strain fields. Comput. Struct. **55**(3), 379–386 (1995)
14. De Souza Neto, E.A., Peric, D., Owen, D.R.J.: Computational Methods for Plasticity: Theory and Applications. Wiley, West Sussex (2008)
15. Dmitrochenko, O., Hussein, B.A., Shabana, A.A.: Coupled deformation modes in the large deformation finite element analysis: generalization. ASME J. Comput. Nonlinear Dyn. **4**(2), 021002-1–021002-8 (2009)
16. Dong, S.B., Alpdogan, C., Taciroglu, E.: Much ado about shear correction factors in Timoshenko beam theory. Int. J. Solids Struct. **47**(13), 1651–1665 (2010)
17. Dorfi, H.R., Busby, H.R.: An effective curved composite beam finite element based on the hybrid-mixed formulation. Comput. Struct. **53**(1), 43–52 (1994)
18. Dufva, K.E., Sopanen, J.T., Mikkola, A.M.: A two-dimensional shear deformable beam element based on absolute nodal coordinate formulation. J. Sound Vib. **280**(3–5), 719–738 (2005)
19. Ebel, H., Matikainen, M.K., Hurskainen, V., Mikkola, A.: Higher-order beam elements based on the absolute nodal coordinate formulation for three-dimensional elasticity. Nonlinear Dyn. **88**(2), 1075–1091 (2016)
20. Ebel, H., Matikainen, M.K., Hurskainen, V., Mikkola, A.: Higher-order plate elements for large deformation analysis in multibody applications. In: Proceedings of the ASME 2016 International Design Engineering Technical Conferences & Computers and Information in Engineering Conference, Charlotte, North Carolina, USA, August 21–24 (2016)
21. Felippa, C.A.: The extended free formulation of finite elements in linear elasticity. ASME J. Appl. Mech. **56**(3), 609–616 (1989)
22. Friedman, Z., Kosmatka, J.B.: An improved two-node Timoshenko beam finite element. Comput. Struct. **47**(3), 473–481 (1993)
23. Garcia-Vallejo, D., Mikkola, A., Escalona, J.L.: A new locking-free shear deformable finite element based on absolute nodal coordinates. Nonlinear Dyn. **50**(1), 249–264 (2007)
24. Gerstmayr, J., Irschik, H.: On the correct representation of bending and axial deformation in the absolute nodal coordinate formulation with an elastic line approach. J. Sound Vib. **318**(3), 461–487 (2008)
25. Gerstmayr, J., Matikainen, M.: Analysis of stress and strain in the absolute nodal coordinate formulation. Mech. Based Des. Struct. Mach. Int. J. **34**(4), 409–430 (2006)
26. Gerstmayr, J., Matikainen, M.K., Mikkola, A.M.: A geometrically exact beam element based on the absolute nodal coordinate formulation. Multibody Sys.Dyn. **20**, 359–384 (2008)
27. Gerstmayr, J., Sugiyama, H., Mikkola, A.: Review on the absolute nodal coordinate formulation for large deformation analysis of multibody systems. ASME J. Comput. Nonlinear Dyn. **8**(3), 031016-1–031016-12 (2013)
28. Hamed, A.M., Jayakumar, P., Letherwood, M.D., Gorsich, D.J., Recuero, A.M., Shabana, A.A.: Ideal compliant joints and integration of computer aided design and analysis. ASME J. Comput. Nonlinear Dyn. **10**(2), 021015-1–021015-14 (2015)
29. Heyliger, P.R., Reddy, J.N.: A higher-order beam finite element for bending and vibration problems. J. Sound Vib. **126**(2), 309–326 (1988)
30. Hughes, T.J.R., Cohen, M., Haroun, M.: Reduced and selective integration techniques in the finite element analysis of plates. Nucl. Eng. Des. **46**(1), 203–222 (1978)
31. Hughes, T.J.R., Taylor, R., Kanoknukulchai, W.: A simple and efficient finite element for plate bending. Int. J. Numer. Methods Eng. **11**(10), 1529–1543 (1977)
32. Hughes, T.J.R.: The Finite Element Method: Linear Static and Dynamic Finite Element Analysis. Prentice Hall, New Jersey (1987)
33. Hurskainen, V.T., Matikainen, M.K., Wang, J., Mikkola, A.M.: A planar beam finite-element formulation with individually interpolated shear deformation. ASME J. Comput. Nonlinear Dyn. **12**(4), 041007-1–041007-8 (2017)

34. Hussein, B.A., Sugiyama, H., Shabana, A.A.: Coupled deformation modes in the large deformation finite-element analysis: problem definition. ASME J. Comput. Nonlinear Dyn. **2**(2), 146–154 (2007)
35. Ibrahimbegovic, A., Wilson, E.L.: A modified method of incompatible modes. Int. J. Numer. Methods Biomed. Eng. **7**(3), 187–194 (1991)
36. Kerkkanen, K.S., Sopanen, J.T., Mikkola, A.M.: A linear beam finite element based on the absolute nodal coordinate formulation. ASME J. Mech. Des. **127**(4), 621–630 (2005)
37. Kim, J.G., Kim, Y.Y.: A new higher-order hybrid-mixed curved beam element. Int. J. Numer. Methods Eng. **43**(5), 925–940 (1998)
38. Kulkarni, S., Pappalardo, C.M., Shabana, A.A.: Pantograph/catenary contact formulations. ASME J. Vib. Acoust. **139**(1), 011010-1–011010-12 (2017)
39. Lee, P., Sin, H.: Locking-free curved beam element based on curvature. Int. J. Numer. Methods Eng. **37**(6), 989–1007 (1994)
40. Liu, W.K., Belytschko, T., Chen, J.: Nonlinear versions of flexurally superconvergent elements. Comput. Methods Appl. Mech. Eng. **71**(3), 241–258 (1988)
41. Liu, C., Tian, Q., Hu, H.: Dynamics of a large scale rigid-flexible multibody system composed of composite laminated plates. Multibody Sys.Dyn. **26**(3), 283–305 (2011)
42. Malkus, D., Hughes, T.J.R.: Mixed finite element methods—reduced and selective integration techniques: a unification of concepts. Comput. Methods Appl. Mech. Eng. **15**(1), 63–81 (1978)
43. Matikainen, M.K., Dmitrochenko, O., Mikkola, A.: Beam elements with trapezoidal cross section deformation modes based on the absolute nodal coordinate formulation. In: International Conference on Numerical Analysis and Applied Mathematics, Rhodes, Greece, September 19–25 (2010)
44. Mikkola, A.M., Matikainen, M.K.: Development of elastic forces for a large deformation plate element based on the absolute nodal coordinate formulation. ASME J. Comput. Nonlinear Dyn. **1**(2), 103–108 (2006)
45. Mikkola, A.M., Shabana, A.A.: A non-incremental finite element procedure for the analysis of large deformation of plates and shells in mechanical system applications. Multibody Syst. Dyn. **9**(3), 283–309 (2003)
46. Mohamed, A.N.A., Liu, J.: The three-dimensional gradient deficient beam element (beam9) using the absolute nodal coordinate formulation. In: Proceedings of the ASME 2014 International Design Engineering Technical Conferences & Computers and Information in Engineering Conference, Buffalo, New York, USA, August 17–20 (2014)
47. Nachbagauer, K.: State of the Art of ANCF elements regarding geometric description, interpolation strategies, definition of elastic forces, validation and locking phenomenon in comparison with proposed beam finite elements. Arch. Comput. Methods Eng. **21**(3), 293–319 (2014)
48. Nachbagauer, K., Gruber, P., Gerstmayr, J.: Structural and continuum mechanics approaches for a 3D shear deformable ANCF beam finite element: application to static and linearized dynamic examples. ASME J. Comput. Nonlinear Dyn. **8**(2), 021004-1–021004-7 (2013)
49. Nachbagauer, K., Gruber, P., Gerstmayr, J.: A 3D shear deformable finite element based on absolute nodal coordinate formulation. Multibody Dyn. Comput. Methods Appl. Sci. **28**, 77–96 (2013)
50. Nachbagauer, K., Pechstein, A.S., Irschik, H., Gerstmayr, J.: A new locking-free formulation for planar, shear deformable, linear and quadratic beam finite elements based on the absolute nodal coordinate formulation. Multibody Syst. Dyn. **26**(3), 245–263 (2011)
51. Noor, A., Peters, J.: Mixed models and reduced/selective integration displacement models for nonlinear analysis of curved beams. Int. J. Numer. Methods Eng. **17**(4), 615–631 (1981)
52. Ogden, R.W.: Nonlinear Elastic Deformations. Ellis Harwood Ltd., Chichester (1984)
53. Olshevskiy, A., Dmitrochenko, O., Kim, C.W.: Three-dimensional solid brick element using slopes in the absolute nodal coordinate formulation. ASME J. Comput. Nonlinear Dyn. **9**(2), 021001-1–021001-10 (2014)
54. Omar, M.A., Shabana, A.A.: A two-dimensional shear deformable beam for large rotation and deformation problems. J. Sound Vib. **243**(3), 565–576 (2001)
55. Orzechowski, G., Fraczek, J.: Nearly incompressible nonlinear material models in the large deformation analysis of beams using ANCF. Nonlinear Dyn. **82**(1), 451–464 (2015)
56. Orzechowski, G., Shabana, A.A.: Analysis of warping deformation modes using higher-order ANCF beam element. J. Sound Vib. **363**, 428–445 (2016)
57. Pappalardo, C.M., Wallin, M., Shabana, A.A.: A new ANCF/CRBF fully-parameterized plate finite element. ASME J. Comput. Nonlinear Dyn. **12**(3), 031008-1–031008-13 (2017)
58. Pappalardo, C.M., Yu, Z., Zhang, X., Shabana, A.A.: Rational ANCF thin plate finite element. ASME J. Comput. Nonlinear Dyn. **11**(5), 051009-1–051009-15 (2016)
59. Patel, M., Orzechowski, G., Tian, Q., Shabana, A.A.: A new multibody system approach for tire modeling using ANCF finite elements. Proc. Inst. Mech. Eng. Park K J. Multibody Dyn. **230**(1), 69–84 (2016)
60. Pian, T.H.H.: Finite elements based on consistently assumed stresses and displacements. Finite Elem. Anal. Des. **1**(2), 131–140 (1985)
61. Pian, T.H.H., Sumihara, K.: Rational approach for assumed stress finite elements. Int. J. Numer. Methods Eng. **20**(9), 1685–1695 (1984)
62. Prathap, G., Babu, R.: Field-consistent strain interpolations for the quadratic shear flexible beam element. Int. J. Numer. Methods Eng. **23**(11), 1973–1984 (1986)
63. Prathap, G., Babu, R.: An isoparametric quadratic thick curved beam element. Int. J. Numer. Methods Eng. **23**(9), 1583–1600 (1984)
64. Prathap, G., Bhashyam, G.R.: Reduced integration and the shear-flexible beam element. Int. J. Numer. Methods Eng. **18**(2), 195–210 (1982)
65. Rakowski, J.: The interpretation of the shear locking in beam elements. Comput. Struct. **37**(5), 769–776 (1990)
66. Rakowski, J.: A critical analysis of quadratic beam finite elements. Int. J. Numer. Methods Eng. **31**(5), 949–966 (1991)

67. Raveendranath, P., Singh, G., Pradhan, B.: A two-noded locking-free shear flexible curved beam element. Int. J. Numer. Methods Eng. **44**(2), 265–280 (1999)
68. Reddy, J.N.: On locking-free shear deformable beam finite elements. Comput. Methods Appl. Mech. Eng. **149**(1–4), 113–132 (1997)
69. Reddy, J.N., Wang, C.M., Lee, K.H.: Relationships between bending solutions of classical and shear deformation beam theories. Int. J. Solids Struct. **34**(26), 3373–3384 (1997)
70. Sanborn, G.G., Choi, J., Choi, J.H.: Curve-induced distortion of polynomial space curves, flat-mapped extension modeling, and their impact on ANCF thin-plate elements. Multibody Syst. Dyn. **26**(2), 191–211 (2011)
71. Sanborn, G.G., Shabana, A.A.: A rational finite element method based on the absolute nodal coordinate formulation. Nonlinear Dyn. **58**, 565–572 (2009)
72. Schwab, A.L., Meijaard, J.P.: Comparison of three-dimensional flexible beam elements for dynamic analysis: finite element method and absolute nodal coordinate formulation. In: Proceedings of ASME International Design Engineering Technical Conferences and Computer and Information in Engineering Conference, Long Beach, CA, September 24–28 (2005)
73. Schwarze, M., Reese, S.: A reduced integration solid-shell finite element based on the EAS and ANS concept—geometrically linear problems. Int. J. Numer. Methods Eng. **80**(10), 1322–1355 (2009)
74. Shabana, A.A.: Definition of the slopes and the finite element absolute nodal coordinate formulation. Multibody Syst. Dyn. **1**(3), 339–348 (1997)
75. Shabana, A.A.: Computational Continuum Mechanics, 3rd edn. Wiley, Chichester (2018)
76. Shabana, A.A.: Dynamics of Multibody Systems, 4th edn. Cambridge University Press, Cambridge (2013)
77. Shen, Z., Li, P., Liu, C., Hu, G.: A finite element beam model including cross-section distortion in the absolute nodal coordinate formulation. Nonlinear Dyn. **77**(3), 1019–1033 (2014)
78. Simo, J.C., Armero, F.: Geometrically non-linear enhanced strain mixed methods and the method of incompatible modes. Int. J. Numer. Methods Eng. **33**(7), 1413–1449 (1992)
79. Simo, J.C., Rifai, M.S.: A class of mixed assumed strain methods and the method of incompatible modes. Int. J. Numer. Methods Eng. **29**(8), 1595–1638 (1990)
80. Simo, J.C., Armero, F., Taylor, R.L.: Improved versions of assumed enhanced strain tri-linear elements for 3D finite deformation problems. Comput. Methods Appl. Mech. Eng. **110**(3–4), 359–386 (1993)
81. Sopanen, J., Mikkola, A.: Studies on the stiffness properties of the absolute nodal coordinate formulation for three-dimensional beams. In: Proceedings Of Design Engineering Technical Conferences & Computers & Information in Engineering Conference, Chicago, Illinois, USA, September 2–6, 2003 (2003)
82. Stolarski, H., Belytschko, T.: On the equivalence of mode decomposition and mixed finite elements based on the Hellinger–Reissner principle. Part 1: theory. Comput. Methods Appl. Mech. Eng. **58**(3), 249–263 (1986)
83. Stolarski, H., Belytschko, T.: On the equivalence of mode decomposition and mixed finite elements based on the Hellinger–Reissner principle. Part 2: applications. Comput. Methods Appl. Mech. Eng. **58**(3), 265–284 (1986)
84. Stolarski, H., Belytschko, T.: Shear and membrane locking in curved C^0 elements. Comput. Methods Appl. Mech. Eng. **41**(3), 279–296 (1983)
85. Stolarski, H., Chen, Y.: Assumed strain formulation for the four-node quadrilateral with improved in-plane bending behavior. Int. J. Numer. Methods Eng. **38**(8), 1287–1305 (1995)
86. Sugiyama, H., Gerstmayr, J., Shabana, A.A.: Deformation modes in the finite element absolute nodal coordinate formulation. J Sound Vib **298**(4–5), 1129–1149 (2006)
87. Sugiyama, H., Koyama, H., Yamashita, H.: Gradient deficient curved beam element using the absolute nodal coordinate formulation. ASME J. Comput. Nonlinear Dyn. **5**(2), 021001-1–021001-8 (2010)
88. Sussman, T., Bathe, K.J.: A finite element formulation for nonlinear incompressible elastic and inelastic analysis. Comput. Struct. **26**(1–2), 357–409 (1987)
89. Sussman, T., Bathe, K.J.: Spurious modes in geometrically nonlinear small displacement finite elements with incompatible modes. Comput. Struct. **140**, 14–22 (2014)
90. Taylor, R.L., Beresford, P.J., Wilson, E.L.: A non-conforming element for stress analysis. Int. J. Numer. Methods Eng. **10**(6), 1211–1219 (1976)
91. Taylor, R.L., Filippou, F.C., Saritas, A., Auricchio, F.: A mixed finite element method for beam and frame problems. Comput. Mech. **31**(1), 192–203 (2003)
92. Tessler, A., Hughes, T.J.R.: An improved treatment of transverse shear in the Mindlin-type four node quadrilateral element. Comput. Methods Appl. Mech. Eng. **39**(3), 311–335 (1983)
93. Timoshenko, S.P.: On the correction for shear of the differential equation for transverse vibrations of prismatic beams. Philos. Mag. **41**, 744–746 (1921)
94. Valkeapää, A.I., Yamashita, H., Jayakumar, P., Sugiyama, H.: On the use of elastic middle surface approach in the large deformation analysis of moderately thick shell structures using absolute nodal coordinate formulation. Nonlinear Dyn. **80**(3), 1133–1146 (2015)
95. Von Dombrowski, S.: Modellierung von Balken bei grossen Verformungen für ein kraftreflektierendes Eingabegerät, Diploma thesis, University Stuttgart & DLR (1997)
96. Wilson, E.L., Taylor, R.L., Doherty, W.P., Ghaboussi, J.: Incompatible displacement models. In: Fenves, J.S., Perrone, N., Robinson, A.R. (eds.) Numerical and Computer Models in Structural Mechanics, pp. 43–57. Academic Press, New York (1973). https://doi.org/10.1016/B978-0-12-253250-4.50008-7
97. Wriggers, P., Reese, S.: A note on enhanced strain methods for large deformations. Comput. Methods Appl. Mech. Eng. **135**(3–4), 201–209 (1996)
98. Yakoub, R.Y., Shabana, A.A.: Three-dimensional absolute nodal coordinate formulation for beam elements: implementation and applications. ASME J. Mech. Des. **123**(4), 614–621 (2001)
99. Yamashita, H., Valkeapää, A.I., Jayakumar, P., Sugiyama, H.: Continuum mechanics based bilinear shear deformable shell element using the absolute nodal coordinate formulation. ASME. J. Comput. Nonlinear Dyn. **10**(5), 051012-1–051012-9 (2015)

100. Yunhua, L.: Explanation and elimination of shear locking and membrane locking with field consistence approach. Comput. Methods Appl. Mech. Eng. **162**(1–4), 249–269 (1998)
101. Zheng, Y., Shabana, A.A.: A two-dimensional shear deformable ANCF consistent rotation-based formulation beam element. Nonlinear Dyn. **87**(2), 1031–1043 (2017)
102. Zienkiewicz, O.C., Owen, D.R.J., Lee, K.N.: Least square-finite element for elasto-static problems. Use of 'reduced' integration. Int. J. Numer. Methods Eng. **8**(2), 341–358 (1974)
103. Zienkiewicz, O.C., Taylor, R., Too, J.M.: Reduced integration technique in general analysis of plates and shells. Int. J. Numer. Methods Eng. **3**(2), 275–290 (1971)